

Iron-peak elements Sc, V, Mn, Cu, and Zn in Galactic bulge globular clusters ^{*}

H. Ernandes¹, B. Barbuy¹, A. Alves-Brito², A. Friaça¹, C. Siqueira-Mello¹, and D. M. Allen¹

¹ Universidade de São Paulo, IAG, Rua do Matão 1226, Cidade Universitária, São Paulo 05508-900, Brazil

² Universidade Federal do Rio Grande do Sul, Departamento de Astronomia, CP 15051, Porto Alegre 91501-970, Brazil

Received ; accepted

ABSTRACT

Aims. Globular clusters are tracers of the history of star formation and chemical enrichment in the early Galaxy. Their abundance pattern can help understanding their chemical enrichment processes. In particular, the iron-peak elements have been relatively little studied so far in the Galactic bulge.

Methods. The main aim of this work is to verify the strength of abundances of iron-peak elements for chemical tagging in view of identifying different stellar populations. Besides, the nucleosynthesis processes that build these elements are complex, therefore observational data can help constraining theoretical models, as well as give hints on the kinds of supernovae that enriched the gas before these stars formed.

Results. The abundances of iron-peak elements are derived for the sample clusters, and compared with bulge field, and thick disk stars. We derive abundances of the iron-peak elements Sc, V, Mn, Cu, and Zn in individual stars of five bulge globular clusters (NGC 6528, NGC 6553, NGC 6522, NGC 6558, HP 1), and of the reference thick disk/inner halo cluster 47 Tucanae (NGC 104). High resolution spectra were obtained with the UVES spectrograph at the Very Large Telescope over the years.

Conclusions. The sample globular clusters studied span metallicities in the range $-1.2 \lesssim [\text{Fe}/\text{H}] \lesssim 0.0$. V and Sc appear to vary in lockstep with Fe, indicating that they are produced in the same supernovae as Fe. We find that Mn is deficient in metal-poor stars, confirming that it is underproduced in massive stars; Mn-over-Fe steadily increases at the higher metallicities due to a metallicity-dependent enrichment by supernovae of type Ia. Cu behaves as a secondary element, indicating its production in a weak-s process in massive stars. Zn has an alpha-like behaviour at low metallicities, which can be explained in terms of nucleosynthesis in hypernovae. At the metal-rich end, Zn decreases with increasing metallicity, similarly to the alpha-elements.

Key words. stars: abundances, atmospheres - Galaxy: bulge – globular clusters: individual (47 Tucanae, NGC 6528, NGC 6553, HP 1, NGC 6522, NGC 6558)

1. Introduction

Chemical tagging is expected to be a key discriminator of chemical evolution processes and stellar populations (e.g. Freeman & Bland-Hawthorn 2002). Among the different groups of chemical elements, alpha-elements, light odd-Z elements and heavy elements are more often studied. The iron-peak elements are less extensively derived, probably because they are formed in more complex processes, and require atomic data, such as hyperfine structure for the odd-Z elements, not always available.

The majority of the iron-peak elements show solar abundance ratios in most objects in the metallicity range

of bulge stars ($[\text{Fe}/\text{H}] \gtrsim -1.5$). There are exceptions, such as the LMC, where Ni, Co, Cr vary in lockstep with Fe, but they are deficient relative to Fe $[\text{Ni}, \text{Co}, \text{Cr}/\text{Fe}] \sim -0.15$ (Pompéia et al. 2008). The elements Sc, Mn, Cu and Zn however show different trends relative to Fe (e.g. Nissen et al. 2000; Ishigaki et al. 2013). In particular, Zn is found to be enhanced in metal-poor halo and thick disk stars in the Milky Way (e.g. Cayrel et al. 2004, Ishigaki et al. 2013), and in dwarf spheroidal galaxies (Skúladóttir et al. 2017). Mn is deficient in metal-poor stars, and increases with metallicity for $[\text{Fe}/\text{H}] \gtrsim -1.0$ (e.g. Cayrel et al. 2004; Ishigaki et al. 2013) for halo and thick disk stars and McWilliam et al. 2003; Sobeck et al. 2006; Barbuy et al. 2013, Schultheis et al. 2017) for bulge stars. The same applies to Cu in field halo, thick disk and bulge stars (Ishigaki et al. 2013; Johnson et al. 2014).

The iron-peak elements include elements with atomic numbers in the range $21 \leq Z \leq 32$, from scandium to ger-

Send offprint requests to: H. Ernandes

^{*} Observations collected both at the European Southern Observatory, Paranal and La Silla, Chile (ESO programmes 65.L-0340 (HP1), 65.L-0371, 67.D-0489 and 69.D-0582, 88.D-0398A (N6522), 93.D-0123A (N6558), 93.D-0124A (HP1))

manium. Sc with $Z=21$ is a transition element between the so-called alpha-elements and the iron-peak elements. They are produced in complex nucleosynthesis processes, such that they can be subdivided in two groups, the lower iron group: $21 \leq Z \leq 26$ including Scandium (Sc), Titanium (Ti), Vanadium (V), Chromium (Cr), Manganese (Mn), Iron (Fe); and the upper iron Group: $27 \leq Z \leq 32$ which includes Cobalt (Co), Nickel (Ni), Copper (Cu), Zinc (Zn), Gallium (Ga) and Germanium (Ge) (Woosley & Weaver 1995, hereafter WW95, Woosley et al. 2002, Woosley, private communication). The lower iron group elements are produced in explosive oxygen burning at temperatures $3 \times 10^9 < T < 4 \times 10^9$ K, explosive Si burning at $4 \times 10^9 < T < 5 \times 10^9$ K, or nuclear statistical equilibrium for $T > 5 \times 10^9$ (WW95, Nomoto et al. 2013). The upper iron group elements are produced in two processes: neutron capture on iron group nuclei during helium burning and later burning stages, and the alpha-rich freezeout from material heated to $> 5 \times 10^9$ K in the deepest layers. The amount of each element ejected at the supernova event depends on the amount of mass that falls back.

There are very few analyses of the odd- Z iron-peak elements Sc, V, Mn, Co, Cu in bulge stars. This may be due to the need to consider hyperfine structure for them and to having only a few reliable lines. McWilliam et al. (2003) derived Mn abundances in 8 bulge field stars. Barbuy et al. (2013, 2015) have derived abundances of Mn, and Zn, for 56 bulge field stars, based on FLAMES-UVES spectra from the Zoccali et al. (2006) sample. Johnson et al. (2014) have derived abundances of the iron-peak elements Cr, Co, Ni, Cu in stars located in bulge field stars using FLAMES-GIRAFFE data by Zoccali et al. (2008), comprising 205 stars in the ($+5^\circ 25', -3^\circ 02'$) field near the globular cluster NGC 6553, and 109 stars in the ($0, -12^\circ$) field. More recently, abundances of iron-peak elements were presented for bulge metal-poor stars by Howes et al. (2014, 2015, 2016), Casey & Schlafman (2015), and Koch et al. (2016). The stars from Howes et al. (2015) that had determined their orbital parameters were selected here as bulge members (their Table 6). As far as we know these data are all that is available presently as concerns bulge stars. Reviews on chemical abundances in the Galactic bulge can be found in McWilliam (2016), and Barbuy et al. (2018).

In the present work we analyse individual stars in the reference globular cluster 47 Tucanae ($[\text{Fe}/\text{H}]^1 = -0.67$, Alves-Brito et al. 2005), and the bulge globular clusters NGC 6553 ($[\text{Fe}/\text{H}] = -0.20$, Alves-Brito et al. 2006), NGC 6528 ($[\text{Fe}/\text{H}] = -0.11$, Zoccali et al. 2004), NGC 6522 ($[\text{Fe}/\text{H}] = -0.95$, Barbuy et al. 2014), HP 1 ($[\text{Fe}/\text{H}] = -1.00$, Barbuy et al. 2006, 2016), and NGC 6558 ($[\text{Fe}/\text{H}] = -1.00$, Barbuy et al. 2017). In previous work we have derived the abundances of the α -elements (O, Mg, Ca, Si, Ti), odd- Z (Na, Al), s-process (Ba, La, Zr), and r-process

(Eu) elements in these clusters. In the present work we derive the abundances of the iron-peak elements Sc, V, Mn, Cu, Zn.

Star clusters are tracers of the formation history of different components of galaxies. Globular clusters are probably the earliest objects to have formed, and they trace the formation of the halo and bulge of our Galaxy (Hansen et al. 2013; Kruijssen 2015; Renzini 2017). As to whether the field stars and globular clusters can be identified as having a same origin, has been a matter of debate in the literature. The detection of abundance anomalies in field stars similar to the anomalies found in globular cluster stars (Gratton et al. 2012) has been used to conclude that at least a fraction of the field stars have their origin in the clusters (Kraft 1983; Martell et al. 2011; Schiavon et al. 2017).

The observations are briefly described in Sect. 2. Line parameters are reported in Sect. 3. Abundance analysis is described in Sect. 4. Results and discussions are presented in Sect. 5. Conclusions are drawn in Sect. 6.

2. Observations

The sample consists of 28 red giant stars, including five in 47 Tucanae (Alves-Brito et al. 2005), four in NGC 6553 (Alves-Brito et al. 2006), three in NGC 6528 (Zoccali et al. 2004), eight in HP 1 (Barbuy et al. 2006, 2016), four in NGC 6522 (Barbuy et al. 2009, 2014), and four in NGC 6558 (Barbuy et al. 2017), all observed with UVES at the 8.2 m Kueyen ESO telescope. The wavelength coverage is 4800-6800 Å. The red portion of the spectrum (5800-6800 Å) was obtained with the ESO CCD # 20, an MIT backside illuminated, of 4096x2048 pixels, and pixel size $15 \times 15 \mu\text{m}$. The blue portion of the spectrum (4800-5800 Å) uses ESO Marlene EEV CCD-44, backside illuminated, 4102x2048 pixels, and pixel size $15 \times 15 \mu\text{m}$. With the UVES standard setup 580, the UVES resolution is $R \sim 45\,000$ for a 1 arcsec slit width, while $R \sim 55\,000$ for a slit of 0.8 arcsec. The pixel scale is $0.0147 \text{ \AA}/\text{pix}$. The log of observations is given in Table 1.

Reductions are described in the references given above, in all cases including bias and inter-order background subtraction, flatfield correction, extraction and wavelength calibration (Ballester et al. 2000). Fig. 1 shows the spectra for some of the program stars around the features studied.

3. Line parameters: hyperfine structure, oscillator strengths, and solar abundances.

To settle suitable values of oscillator strengths and central wavelengths, the studied lines were checked by using high-resolution spectra of the Sun (using the same instrument settings as the present sample of spectra²), Arcturus (Hinkle et al. 2000) and the metal-rich giant star μ Leo (Lecureur et al. 2007). We adopted the stellar parameters

¹ We adopted here the usual spectroscopic notation that $[A/B] = \log(N_A/N_B)_* - \log(N_A/N_B)_\odot$ and $\epsilon(A) = \log(N_A/N_B) + 12$ for each elements A and B.

² http://www.eso.org/observing/dfp/quality/UVES/-pipeline/solar_spectrum.html

Table 1: Log of spectroscopic observations of globular clusters, 47 Tucanae, NGC 6553, NGC 6528, HP 1, NGC 6558.

Star	Slit width	(S/N)/px
47 Tucanae		
M8	0.8''	280
M11	0.8''	241
M12	0.8''	247
M21	0.8''	213
M25	0.8''	258
NGC 6553		
II-64	0.8''	110
II-85	0.8''	200
III-8	0.8''	170
267092	0.8''	110
NGC 6528		
I-18	1.0''	40
I-36	1.0''	40
II-42	0.8''	30
HP 1		
2	0.8''	70
3	0.8''	45
2115	0.8''	> 200
2461	0.8''	> 200
2939	0.8''	> 200
3514	0.8''	> 200
5037	0.8''	> 200
5485	0.8''	> 200
NGC 6522		
B-107	0.9''	180
B-122	0.9''	170
B-128	0.9''	180
B-130	0.9''	210
NGC 6558		
283	1.0''	130
364	1.0''	150
1072	1.0''	190
1160	1.0''	170

effective temperature (T_{eff}), surface gravity ($\log g$), metallicity ($[\text{Fe}/\text{H}]$) and microturbulent velocity (v_t) of (4275 K, 1.55, -0.54, 1.65 km.s⁻¹) for Arcturus from Meléndez et al. (2003), and (4540 K, 2.3, +0.30, 1.3 km.s⁻¹) for μ Leo from Lecureur et al. (2007). In Table 2, we present the adopted abundances for the Sun, Arcturus and μ Leo.

Oscillator strengths for Sc I, Sc II, V I, and Cu I reported in Table A.2, are from Kurucz (1993)³, NIST (Martin et al. 2002)⁴, VALD3 (Piskunov et al. 1995)⁵, literature values, and adopted final values.

3.1. Scandium and Vanadium

⁴⁵Sc is the unique species of Sc, and the V abundance corresponds to 99.75% of ⁵¹V and 0.25% of ⁵⁰V (Asplund et al. 2009), therefore we adopted ⁵¹V as unique isotope. We selected Sc I, Sc II, and V I lines that showed to be

³ <http://kurucz.harvard.edu/atoms.html>

⁴ http://physics.nist.gov/PhysRefData/ASD/lines_form.html

⁵ <http://vald.astro.univie.ac.at>

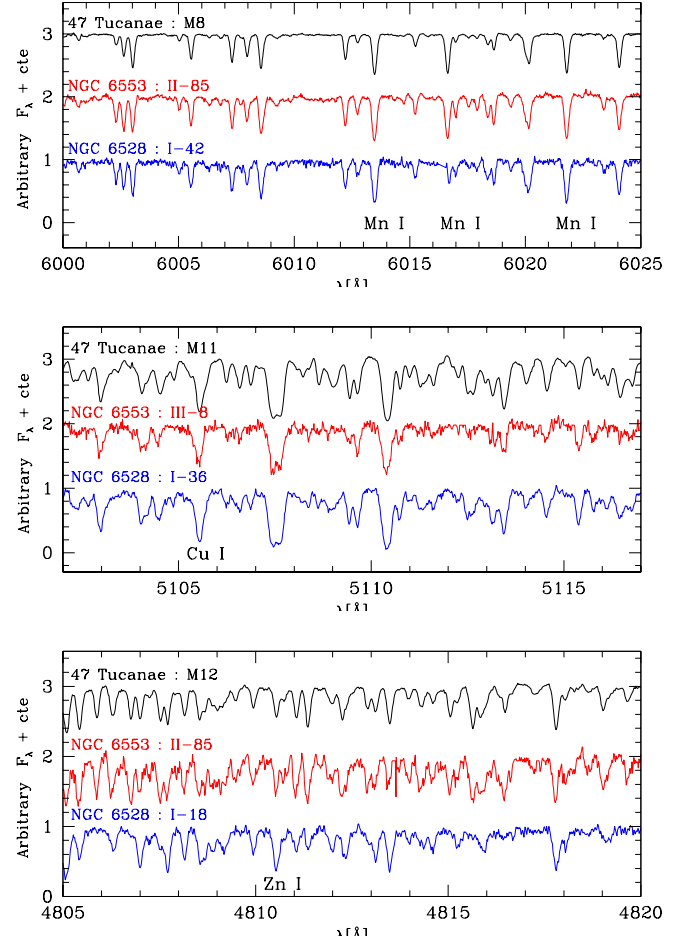


Fig. 1: Comparison of the spectra for each globular cluster in the sample. The features are marked for Mn I (*top*), Cu I (*middle*), and Zn I lines (*bottom*).

strong enough to be detected in red giants. Hyperfine structure (HFS) was taken into account, by applying the code made available by McWilliam et al. (2013), together with the A, and B constants reported in Table A.1. V and Sc have a nuclear spin $I = 7/2$. Some lines that were blended in the sample stars, or affected by telluric lines, were discarded. This applies to the lines V I 4831.640, 4851.480, 4875.480, 4932.030, 5627.640, 5670.850, 6216.370, and 6285.160 Å.

3.2. Copper

The isotopic fractions of 0.6894 for ⁶³Cu and 0.3106 for ⁶⁵Cu (Asplund et al. 2009) are considered. Copper abundances were derived from the Cu I lines at 5105.50 Å and 5218.20 Å. The 5782 Å line is not available in the UVES spectra analysed, which cover the wavelengths 4780-5775 Å and 5817-6821 Å, therefore with a gap of about 40 Å in the range 5775-5817 Å. Oscillator strengths of the Cu I

Table 2: Adopted abundances for the Sun, Arcturus, and μ Leo. References: [1]: Grevesse et al. (1996); [2]: Allende Prieto et al. (2001); [3]: Ramírez & Allende Prieto (2011); [4]: Meléndez et al. (2003) [5]: this work; [6]: Barbuy et al. (2015); [7]: Fulbright et al. (2007); [8]: Smith et al. (2013); [9]: Gratton & Sneden (1990); [10]: Steffen et al. (2015).

El.	$A(X)_{\odot}$	$A(X)_{Arcturus}$	$A(X)_{\mu Leo}$
Fe	7.50 [1]	6.96 [4]	7.80 [6]
C	8.55 [1]	8.32 [3]	8.55 [6]
N	7.97 [1]	7.68 [4]	8.83 [6]
O	8.76 [10]	8.66 [4]	8.97 [6]
Na	6.33 [1]	5.82 [3]	7.06 [7]
Mg	7.58 [1]	7.47 [3]	7.85 [8]
Al	6.47 [1]	6.26 [3]	6.90 [8]
Si	7.55 [1]	7.30 [3]	7.76 [8]
K	5.12 [1]	4.99 [3]	5.63 [8]
Ca	6.36 [1]	5.94 [3]	6.62 [8]
Sc	3.17 [1]	2.81 [3]	3.34 [9]
Ti	5.02 [1]	4.66 [3]	5.40 [8]
V	4.00 [1]	3.58 [3]	4.18 [8]
Cr	5.67 [1]	4.99 [3]	6.14 [8]
Mn	5.39 [1]	4.74 [3]	5.79 [8]
Co	4.92 [1]	4.71 [3]	5.23 [8]
Ni	6.25 [1]	5.73 [4]	6.60 [8]
Cu	4.21 [1]	3.67 [5]	4.46 [5]
Zn	4.60 [1]	4.06 [6]	4.80 [6]

lines were selected in the literature from Kurucz (1993), Bielski (1975), NIST or VALD, and the final adopted values are reported in Table A.2.

In Table A.1 the magnetic dipole A-factor and the electric quadrupole B-factor constants were adopted from Kurucz (1993), and Biehl (1976), in order to compute HFS. For the 5218 Å line the constants for the 4d 2D level are not available. According to R. Kurucz (private communication), the upper level should have much smaller HFS than the lower, because its wavefunction is further away from the nucleus, and setting its splitting to 0.0 is acceptable. The HFS components for the CuI lines and corresponding oscillator strengths are reported in Table A.3.

The CuI 5105 Å and CuI 5218 Å lines in the solar spectrum were fitted adopting $A(\text{Cu})_{\odot} = 4.21$ (Grevesse et al. 1996) cf. Table 2. The adopted or derived abundances for each of the reference stars are also presented in Table 2, corresponding to $[\text{Cu}/\text{Fe}] = 0.0$ and $+0.05$ in Arcturus and μ Leo, respectively.

Figure 2 shows the fits to the solar, Arcturus, and μ Leo spectra for the Cu lines. For the CuI 5218 Å in Arcturus, an asymmetry remained in the blue wing of the Fe profile close to the CuI line. Consequently, the CuI 5218 Å line was used in the sample stars with caution.

3.3. Manganese and Zinc

Manganese has one isotope ^{55}Mn and, for zinc, $^{64,66,68}\text{Zn}$ are the dominant species with 48.63/27.90/18.75% frac-

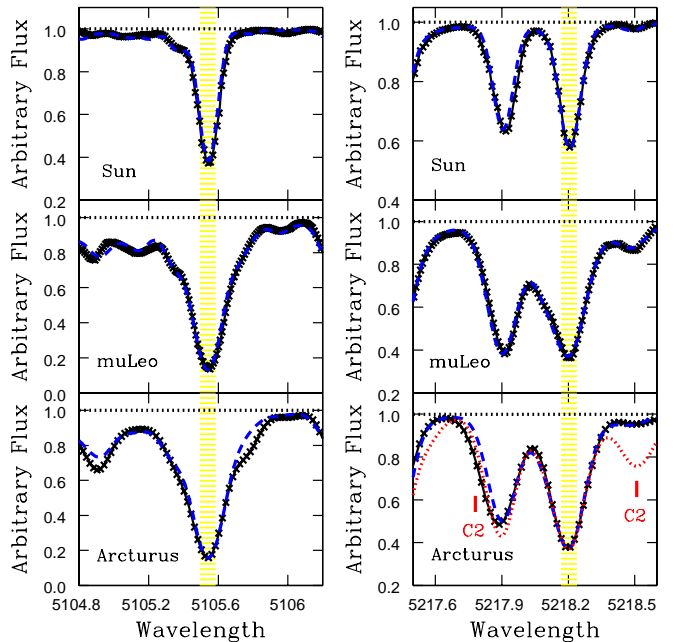


Fig. 2: Fittings on solar, Arcturus, and μ Leo spectra for the CuI lines at 5105 Å and 5218 Å (yellow lines). Observations (black crosses) are compared with synthetic spectra computed using the adopted abundances (dashed blue lines).

tions (Asplund et al. 2009). For these elements a splitting in isotopes was not considered. Manganese abundances were derived from the MnI triplet lines at 6013.513, 6016.640, 6021.800 Å. The line list of HFS components are given in Barbuy et al. (2013). For zinc we used the ZnI 4810.529 and 6362.339 Å lines as detailed in Barbuy et al. (2015).

4. Abundance Analysis

4.1. Atmospheric parameters and abundance derivation

The adopted effective stellar atmospheric parameters for all program stars were derived in previous work (Zoccali et al. 2004; Alves-Brito et al. 2005; Alves-Brito et al. 2006; Barbuy et al. 2006, 2014, 2016, 2017 (in prep.)).

The method described in the original papers follow standard procedures:

- i Colours V-I, V-K, and J-K, corrected by the reddening values reported in Table 3, were used together with colour-temperature calibrations by Alonso et al. (1999, 2001), and/or Houdashelt et al. (2000).
- ii Gravities of the sample stars were obtained adopting the classical relation below, and final log g values were obtained from ionization equilibrium of Fe I and Fe II lines.

$$\log g_* = 4.44 + 4 \log \frac{T_*}{T_{\odot}} + 0.4(M_{\text{bol}*} - M_{\text{bol}\odot}) + \log \frac{M_*}{M_{\odot}} \quad (1)$$

Table 3: Reddening and distance moduli adopted. References: 1 Harris (1996); 2 Zoccali et al. (2001a); 3 Zoccali et al. (2004); 4 Barbuy et al. (1998); 5 Guarnieri et al. (1998); 6 Barbuy et al. (2006); 7 Ortolani et al. (2007, 2011); 8 Barbuy et al. (2009); 9 Terndrup (1988); 10 Rossi et al. (2015).

Cluster	E(B-V)	Ref. $(m - M)_0$	Ref.
47 Tucanae	0.04	1	13.09 2
NGC 6528	0.46	3	14.45 4
NGC 6553	0.70	5	13.54 4
HP 1	1.12	6	14.15 7
NGC 6522	0.45	8	13.91 4
NGC 6558	0.38	9	14.43 10

We adopted $T_{\odot} = 5770$ K and $M_{\text{bol}\odot} = 4.75$ for the Sun and $M_{*} = 0.80$ to $0.88 M_{\odot}$ for the red giant branch (RGB) stars.

In Table 3 are reported the distance moduli assumed for each sample cluster and corresponding references.

- iii The initial photometric temperatures and gravities were used to compute the excitation and ionization equilibrium. Effective temperatures were then checked by imposing excitation equilibrium for FeI and FeII lines of different excitation potential, and gravities were checked against ionization equilibrium.
- iv Microturbulent velocity v_t was determined by canceling any trend in a FeI abundance versus equivalent width diagram.
- v Finally, the metallicities for the sample were derived using a set of equivalent widths of Fe I and Fe II lines.

Table 4 summarizes the final atmospheric parameters obtained for the program stars. In this Table we also present carbon, nitrogen and oxygen abundance ratios, derived from the $C_2(0,1)$ $A^3\Pi-X^3\Pi$ bandhead at 5635.3 \AA , $CN(5,1)$ $A^2\Pi-X^2\Sigma$ 6332.18 and the forbidden $[OI]$ 6300.311 \AA lines.

Elemental abundances were obtained through line-by-line spectrum synthesis calculations. The calculations of synthetic spectra were carried out using the code described in Barbuy et al. (2003), and Coelho et al. (2005). Atomic lines are as described in Sect. 3.2, and molecular lines of CN $A^2\Pi-X^2\Sigma$, C_2 Swan $A^3\Pi-X^3\Pi$ and TiO $A^3\Phi-X^3\Delta$ γ and $B^3\Pi-X^3\Delta$ γ' systems are taken into account. The atmospheric models were obtained by interpolation in the grid of MARCS LTE models (Gustafsson et al. 2008), adopting their spherical and mildly CN-cycled ($[C/Fe] = -0.13$, $[N/Fe] = +0.31$) subgrid. These models consider $[\alpha/Fe] = +0.20$ for $[Fe/H] = -0.50$ and $[\alpha/Fe] = +0.40$ for $[Fe/H] \leq -1.00$.

In Figures 3a,b,c and 4a,b are shown examples of fitting of synthetic spectra to the observed lines.

4.2. Uncertainties

The final adopted atmospheric parameters for all program stars were based on Fe I and Fe II lines in the papers cited

above, and we have adopted their estimated uncertainties in the atmospheric parameters, i.e., ± 100 K for temperature, ± 0.20 for surface gravity, ± 0.10 dex for $[Fe/H]$ and $\pm 0.20 \text{ kms}^{-1}$ for microturbulent velocity. In Table 5 the final uncertainties in the abundances of the iron-peak elements studied are reported for the metal-poor star HP-1:2115, and the metal-rich star NGC 6528:I36. Given that the stellar parameters are correlated among them, the covariance will be non-zero. Since we have taken into account only the diagonal terms of the covariance matrix, these errors are overestimated.

In order to further inspect the errors in stellar parameters, we applied NLTE corrections to abundances as given in Lind et al. (2012), and following suggestions given in Bergemann et al. (2013). For star HP1-2939 as an example, we show the LTE excitation and ionization potential plots in Fig. 5, restricting to lines with excitation potential $\chi_{ex} \geq 2.0$ eV. We then applied a) the NLTE abundance correction to each FeI line, and ran the excitation and ionization equilibrium once more. This is shown in Fig. 6a (left panel). The result is a negligible change in metallicity from Fe I lines of about 0.015 dex.

b) the NLTE correction on gravity $\log g$, amounting to $\Delta \log g = 0.04$ - see Fig. 6b (right panel). It can be seen that the difference in metallicity between Fe I and Fe II increased to 0.02 instead of the previous 0.01 difference.

c) the NLTE correction on temperature is negligible (6 K)

d) the NLTE on microturbulence velocity is also negligible at these metallicities.

As shown in Fig. 6 by Bergemann et al. (2013), the effects are not pronounced for stars of metallicity $[Fe/H] \gtrsim -1.0$, therefore they can be neglected for the present sample stars, given the other larger errors.

We also have to take into account errors on S/N and equivalent widths. These errors are given by the Cayrel (1988) formula (see also Cayrel et al. 2004) $\sigma = \frac{1.5}{S/N} \sqrt{FWHM * \delta x}$. Adopting a mean FWHM = 12.5 pixels, or 0.184 \AA . The CCD pixel size is $15 \mu\text{m}$, or $\delta x = 0.0147 \text{ \AA}$ in the spectra. By assuming a mean S/N=100, we derive an error $\Delta EW \sim 0.8 \text{ m\AA}$ (note that this formula neglects the uncertainty in the continuum placement).

In order to take the S/N and fitting error into account, we adopt $\delta_{noise} = \frac{\sigma}{\sqrt{N-1}}$. These are reported in Table 7.

The final error is given by the equation $\delta_{[X/Fe]} = \sqrt{\delta_{noise}^2 + \delta_{parameters}^2}$ where for the error on stellar parameters the values given in Table 5 for the metal-poor stars HP1:2115 are applied to the stars more metal-poor than $[Fe/H] < -0.5$, and those for NGC 6528:I36 to the metal-rich stars.

5. Results and discussions

Very few abundances are available for iron-peak elements in bulge stars. In this Section, we present results and discuss the available chemical evolution models, and associated nucleosynthesis of the studied species. We have

Table 4: Atmospheric parameters adopted.

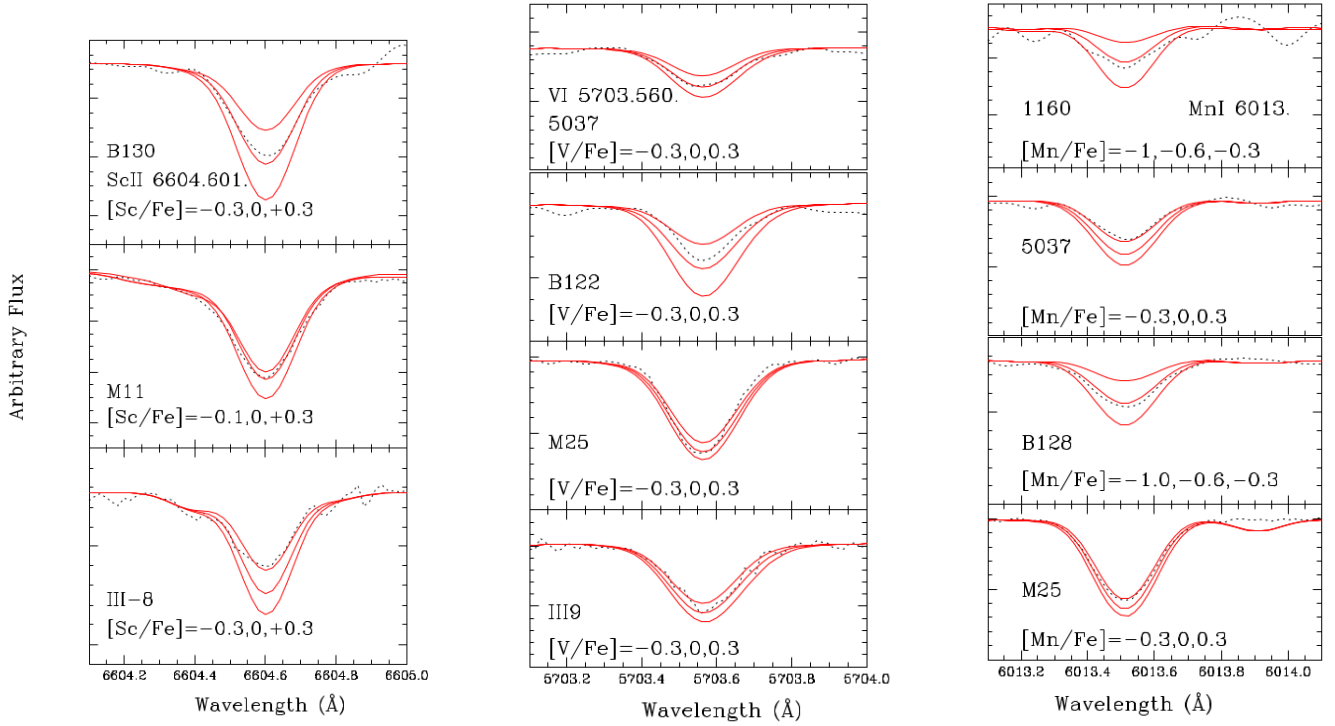
Star (1)	T_{eff} [K] (2)	$\log g$ (3)	[FeI/H] (4)	[FeII/H] (5)	[Fe/H] (6)	v_t [kms $^{-1}$] (7)	[C/Fe] (8)	[N/Fe] (9)	[O/Fe] (10)
47 Tucanae									
M8	4086	1.48	-0.62	-0.65	-0.64	+1.42	+0.20	+0.50	+0.45
M11	3945	1.20	-0.62	-0.62	-0.62	+1.49	+0.00	+0.50	+0.25
M12	4047	1.45	-0.63	-0.68	-0.66	+1.45	+0.00	+0.50	+0.45
M21	5100	2.46	-0.77	-0.82	-0.80	+1.42	+0.20	+0.50	+0.30
M25	4200	1.65	-0.64	-0.67	-0.66	+1.37	-0.10	+0.20	+0.35
NGC 6553									
II-64	4500	2.20	-0.20	-0.20	-0.20	+1.45	+0.00	+0.50	+0.45
II-85	3800	1.10	-0.23	-0.29	-0.26	+1.38	+0.00	+0.50	+0.30
III-8	4600	2.40	-0.17	-0.17	-0.17	+1.40	+0.00	+0.50	+0.30
267092	4600	2.50	-0.21	-0.22	-0.22	+1.50	+0.00	+1.00	—
NGC 6528									
I-18	4700	2.00	-0.05	-0.11	-0.08	+1.50	-0.20	+0.30	+0.30
I-36	4200	1.50	-0.13	-0.09	-0.11	+1.50	-0.30	+0.80	+0.00
I-42	4100	1.60	-0.14	-0.08	-0.11	+1.20	+0.00	+0.20	+0.05
HP 1									
HP 1-2	4630	1.70	-1.02	-0.97	-1.00	+1.60	+0.00	+0.20	+0.30
HP 1-3	4450	1.75	-0.99	-0.95	-0.97	+ 1.40	+0.00	+0.20	+0.30
2115	4530	2.00	-0.98	-1.02	-1.00	+ 1.45	+0.00	+0.70	+0.40
2461	4780	2.05	-1.13	-1.09	-1.11	+ 1.90	+ 0.00	+0.50	+0.50
2939	4525	2.00	-1.07	-1.07	-1.07	+ 1.65	+0.00	+0.50	+0.50
3514	4560	1.80	-1.18	-1.19	-1.18	+ 2.00	+0.00	+0.80	+0.40
5037	4570	2.15	-0.98	-1.03	-1.00	+ 1.20	+0.00	+0.50	+0.35
5485	4920	2.07	-1.18	-1.18	-1.18	+ 1.80	+0.00	+0.50	+0.40
NGC 6522									
B-107	4990	2.00	-1.11	-1.14	-1.13	+ 1.40	+0.00	+0.70	+0.30
B-122	4900	2.70	-0.80	-0.82	-0.81	+1.55	-0.20	+0.70	+0.40
B-128	4800	2.50	-0.81	-0.82	-0.82	+1.25	+0.10	+0.70	+0.50
B-130	4850	2.20	-1.03	-1.04	-1.04	+1.45	+0.10	+0.70	+0.50
NGC 6558									
283	4840	2.50	-1.14	-1.16	-1.15	+1.05	+0.10:	+0.70	+0.50
364	4880	2.35	-1.18	-1.13	-1.15	+1.90	+0.10	+0.80	+0.20
1160	4890	2.35	-1.03	-1.04	-1.04	+0.73	+0.20	+1.00	+0.50
1072	4850	2.60	-1.20	-1.26	-1.23	+1.10	+0.10	+1.00	+0.55

included all chemical evolution models available for the Galactic bulge for these elements.

The abundances of Sc I, Sc II, V I, Mn I, Cu I, and Zn I for each sample star are listed in Table 6. In Figures 7, 8, 9, 11, 13 we plot the element-to-iron ratio versus the metallicity [Fe/H].

5.1. Scandium, Vanadium and Manganese

Sc is intermediate between the alpha-elements and the iron-peak elements. ^{45}Sc is produced in central He burning and in C-burning shell, in a so-called weak-s process, and during neon burning and as the radioactive progenitor ^{45}Ti in explosive oxygen and silicon burning (WW95,LC03). V, Cr, Mn are mainly produced in incomplete explosive Si burning in outer layers of massive stars (WW95, Limongi & Chieffi 2003, hereafter LC03).

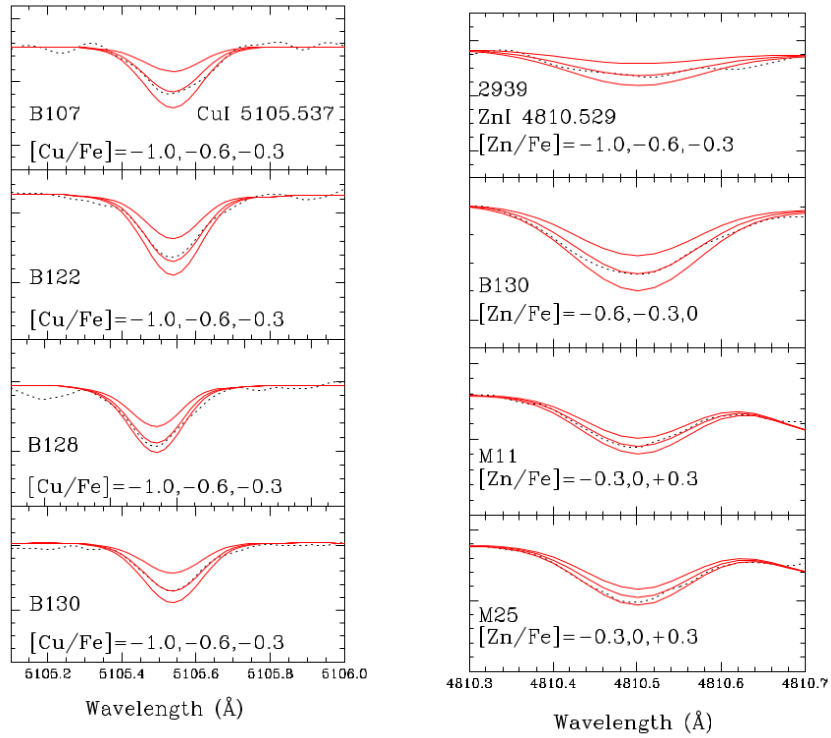


(a) Sc I 6604.601 Å line.

(b) VI 5703.560 Å line.

(c) Mn I 6013.513 Å line.

Fig. 3: Fits of best lines of Sc I, VI, and Mn I for some sample stars.



(a) Cu I 5105.537 Å line.

(b) Zn I 4810.529 Å line.

Fig. 4: Fits of best lines of Cu I and Zn I for some sample stars.

Table 5: Sensitivity of abundances to changes of $\Delta T_{\text{eff}} = 100$ K, $\Delta \log g = +0.20$, $\Delta[\text{Fe}/\text{H}] = +0.1$, and $\Delta v_t = 0.20$ km s $^{-1}$. In the last column the corresponding total error is given.

Species	ΔT (100 K)	$\Delta \log g$ (+0.20 dex)	$\Delta[\text{Fe}/\text{H}]$ (+0.10 dex)	Δv_t (+0.20 kms $^{-1}$)	$(\sum x^2)^{1/2}$
(1)	(2)	(3)	(4)	(5)	(6)
HP 1 : 2115					
[Sc/Fe]	-0.02	+0.10	-0.010	-0.01	+0.10
[V/Fe]	+0.15	+0.01	-0.015	-0.01	+0.15
[MnI/Fe]	+0.01	+0.01	-0.010	-0.02	+0.03
[CuI/Fe]	+0.10	+0.02	-0.005	-0.10	+0.14
[ZnI/Fe]	-0.05	+0.10	-0.030	-0.01	+0.12
NGC 6528 : I-36					
[Sc/Fe]	-0.02	+0.10	-0.030	-0.05	+0.12
[V/Fe]	+0.05	+0.01	-0.020	-0.12	+0.13
[MnI/Fe]	+0.01	+0.01	-0.015	-0.10	+0.10
[CuI/Fe]	+0.02	+0.01	-0.010	-0.12	+0.12
[ZnI/Fe]	+0.07	+0.07	-0.050	-0.15	+0.19

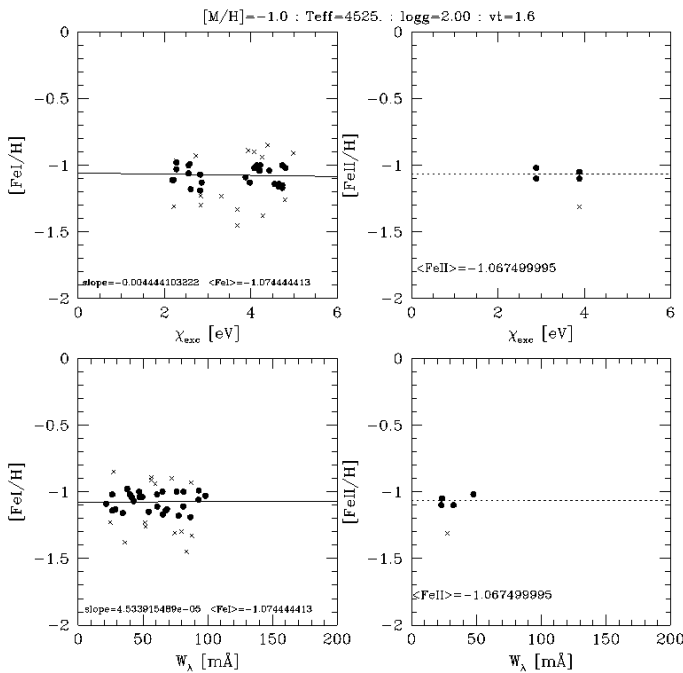


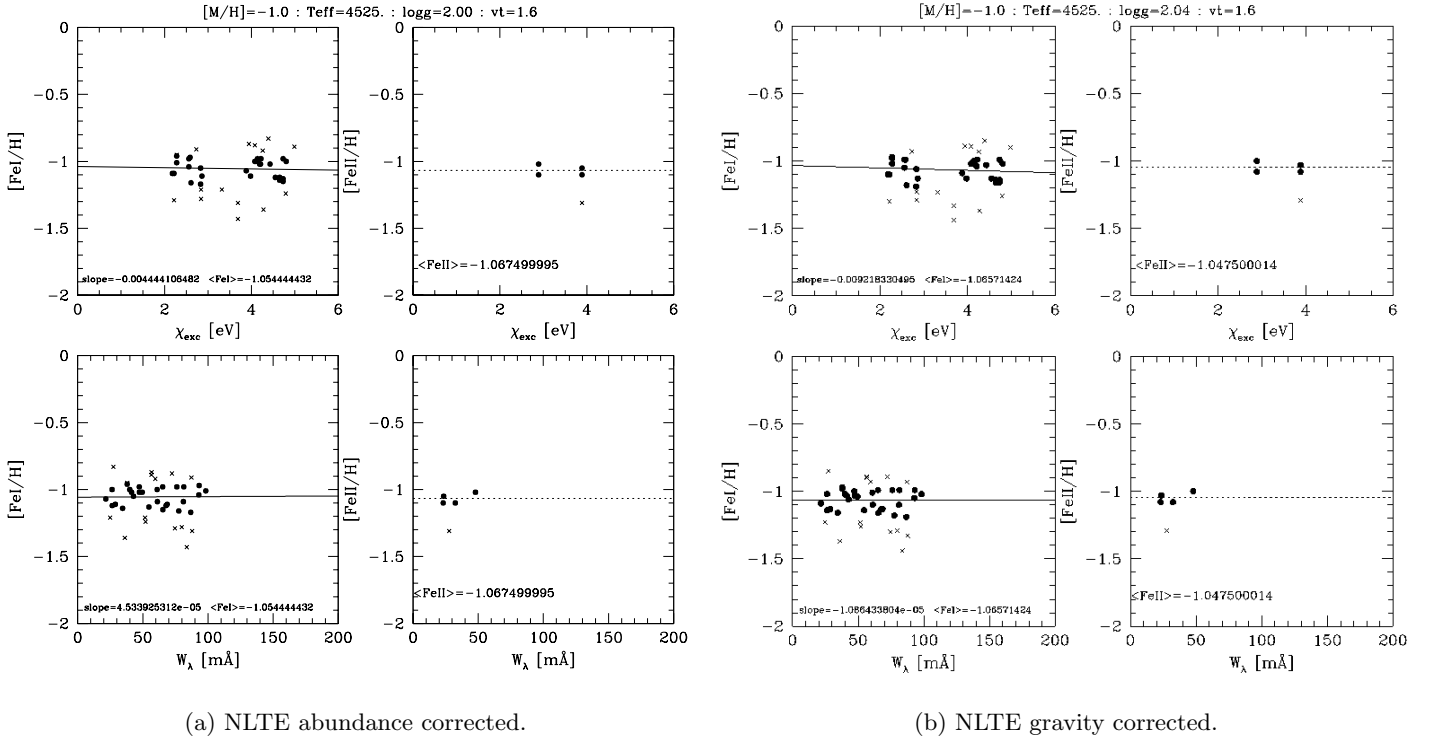
Fig. 5: Excitation and ionization equilibria of FeI and FeII lines for star 2939 in LTE.

Fig. 7 compares the present $[\text{Sc}/\text{Fe}]$ values with metal-poor bulge stars by Howes (2015, 2016) for thick disk and halo stars by Nissen et al. (2000) and Ishigaki et al. (2013) and thin and thick disk stars by Battistini & Bensby (2015). The data show a considerable spread, but it is possible to interpret the metal-poor side from Howes et al. and Ishigaki et al. as somewhat enhanced with $[\text{Sc}/\text{Fe}] \sim 0.2$. Fishlock et al. (2017) confirm the findings by Nissen et al. (2000), that high- and low-alpha halo stars show high

and low Sc abundances respectively. Data by Nissen et al. (2000) tend to show a trend of decreasing $[\text{Sc}/\text{Fe}]$ with increasing metallicity. Contrarily to the Sc enhancement in the more metal-poor stars from Howes et al. (2015, 2016), the present results on moderately metal-poor bulge clusters do not show a significant Sc enhancement. Our results are lower than Nissen et al. (2000)'s values, and fit well the level of $[\text{Sc}/\text{Fe}]$ values by Battistini & Bensby (2015) for thin and thick disk stars. The metal-rich globular clusters NGC 6528 and NGC 6553 show a spread in Sc abundances at $[\text{Fe}/\text{H}] \sim -0.2$, that might be considered as a decrease with increasing metallicity at the high metallicity end.

Figure 8 shows that V varies in lockstep with Fe. There are no V abundances for bulge stars other than the present data. The thin and thick disk data from Reddy et al. (2003, 2006) are overplotted. The thick disk V abundances from Reddy et al. (2006) appear to be enhanced with respect to thin disk stars (Reddy et al. 2003), as well as to the present results, whereas they seem to be at the same level as thin and thick disk stars by Battistini & Bensby (2015). For the more metal-rich stars the bulge globular cluster stars tend to decrease with increasing metallicity, which could be due to enrichment in Fe by SNIa. Due to uncertainties, the spread in the data do now allow to derive further conclusions from V abundances.

Kobayashi et al. (2006, hereafter K06) have shown that Sc, and V yields are underabundant by 1 dex based on previous nucleosynthesis prescriptions. Umeda & Nomoto (2005, hereafter UN05), Kobayashi et al. (2006), Nomoto et al. (2013) have introduced a low-density model, during explosive burning, enhancing Sc abundance through the alpha-rich freezeout. Yoshida et al. (2008) applied a ν -process to Si explosive nucleosynthesis, producing larger amounts of Sc, V, and Mn production by a factor of 10. Fröhlich et al. (2006) showed that a delayed neutrino mechanism leading to an electron fraction value of $Y_e \gtrsim$



(a) NLTE abundance corrected.

(b) NLTE gravity corrected.

Fig. 6: Excitation and ionization equilibria of Fe I and Fe II lines for star 2939. a) applying NLTE abundance correction; b) applying NLTE gravity correction.

0.5 in the innermost region gives larger production of Sc, Ti and Zn. In conclusion, given that the available models do not reproduce the observations (Kobayashi et al. 2006) for both Sc and V, due to low yields from nucleosynthesis yields, these models are not overplotted to the data.

Figure 9 shows $[\text{Mn}/\text{Fe}]$ vs. $[\text{Fe}/\text{H}]$ for the present results, together with previous results in Galactic bulge stars measured by McWilliam et al. (2003), Barbuy et al. (2013), and Schultheis et al. (2017), and results for thin and thick disk stars by Battistini & Bensby (2015). It is important to note that NLTE corrections in the range of parameters of the present data are small (Bergemann & Gehren 2008). The only available bulge chemical evolution models by Cescutti et al. (2008) and Kobayashi et al. (2006) are overplotted. Cescutti et al. (2008) computed models for Mn enrichment in the Galactic bulge, adopting a star formation rate 20 times faster than in the solar neighbourhood, and a flatter IMF. Their preferred model adopts metallicity dependent yields from WW95 for massive stars, and Iwamoto et al. (1999) for intermediate mass stars. K06 produced a grid of yields, including both SNI and hypernovae, and further have built chemical evolution models for Galaxy components, including the bulge.

The present Mn abundances in globular cluster stars follow the trend of field stars, i.e., with $[\text{Mn}/\text{Fe}] \sim 0.5$ at $[\text{Fe}/\text{H}] \sim 1.5$, increasing steadily with increasing metallicity, and they are well reproduced by the models.

Finally, Fig. 10 shows $[\text{Mn}/\text{O}]$ vs. $[\text{Fe}/\text{H}]$, revealing differences between thin, thick and bulge stars, as previously

pointed out by Feltzing et al. (2007) and Barbuy et al. (2013). This is of great importance since $[\text{Mn}/\text{O}]$ can be used as a discriminator between different stellar populations, that otherwise have a similar behaviour.

5.2. Copper

$^{63,65}\text{Cu}$ are mainly produced through neutron-capture during core He burning and convective shell carbon burning, therefore Cu may be classified as produced in a weak s-process component (LC03). Some primary ^{65}Cu is also made as ^{65}Zn in explosive nucleosynthesis through alpha-rich freezeout (WW95, Pignatari et al. 2010). Cu is not significantly produced in SNIa, nor in AGB stars or through the r-process (Pignatari et al. 2010).

Johnson et al. (2014) derived copper abundances for a large sample of bulge red giants. Their results show a low Cu abundance ratio at low metallicities that increases with increasing $[\text{Fe}/\text{H}]$. For supersolar metallicities, $[\text{Cu}/\text{Fe}]$ values appear to be enhanced relative to other stellar populations.

The present results are plotted in Fig. 11, together with data from Johnson et al. (2014) for the bulge, and Ishigaki et al. (2013) for the thick disk. Our results tend to be less enhanced than those by Johnson et al. (2014). There is good agreement between the data and the models by Kobayashi et al. (2006). The metal-poor clusters show very low $[\text{Cu}/\text{Fe}]$.

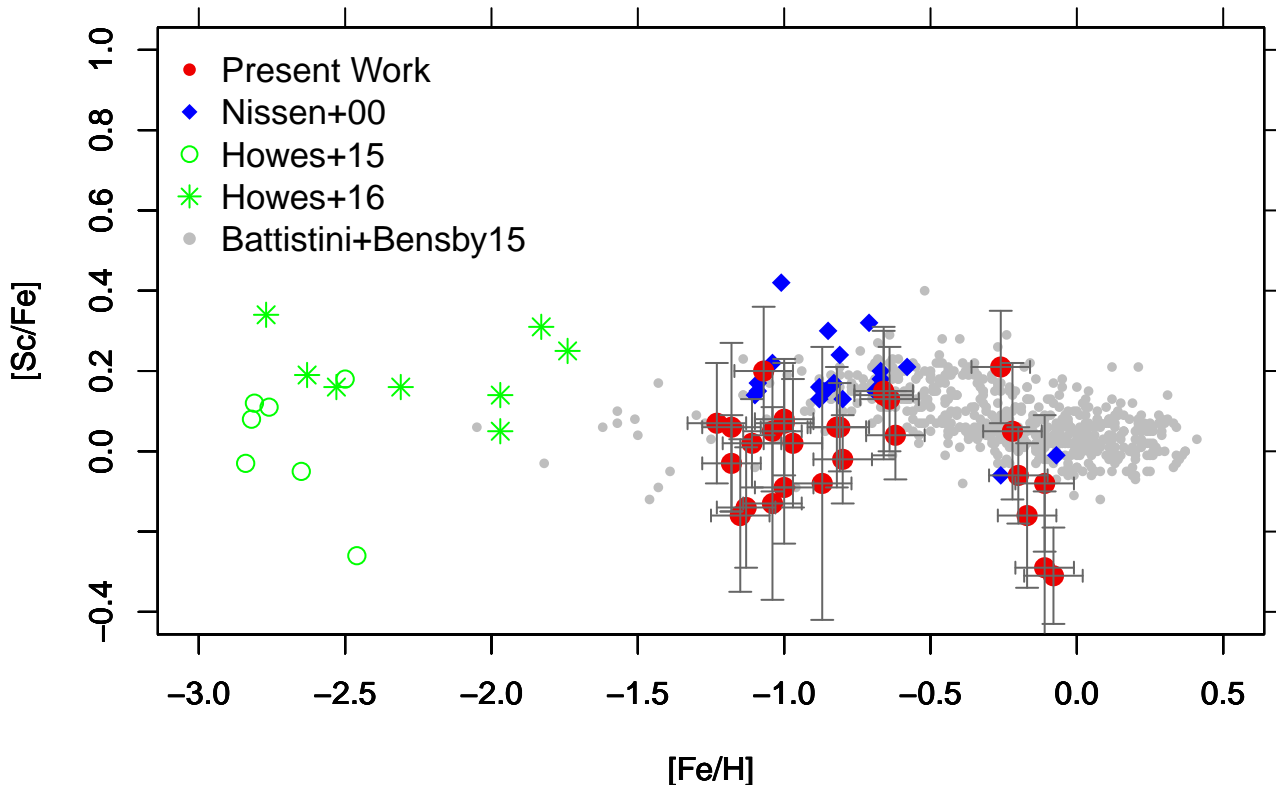


Fig. 7: $[\text{Sc}/\text{Fe}]$ vs. $[\text{Fe}/\text{H}]$. Symbols: present work (filled red circles), Bensby et al. (2017) (black filled circles), Nissen et al. (2000) (filled blue diamonds), Howes et al. (2015) (open green circles), Howes et al. (2016) (green crosses); Battistini & Bensby (2015) (grey filled circles). Error bars on $[\text{Sc}/\text{Fe}]$ are indicated. Errors on $[\text{Fe}/\text{H}]$ can be assumed as constant, of the order of $\Delta[\text{Fe}/\text{H}]=\pm 0.17$ dex.

According to McWilliam (2016) $[\text{Cu}/\text{O}]$ has much less spread than $[\text{Cu}/\text{Fe}]$ data, Fig. 12 shows $[\text{Cu}/\text{O}]$ vs. $[\text{Fe}/\text{H}]$, where the behaviour of the sample cluster stars track well the Johnson et al. (2014) field stars data. This rather straight correlation between Cu and O, indicates the production of Cu and O in the same massive stars.

5.3. Zinc

The main isotopes of Ti, Co, Ni, Cu, Zn are produced only or mainly in the zone that undergoes explosive Si burning with complete Si exhaustion (LC03). The relevant Zn isotopes $^{64,66,67,68}\text{Zn}$ are produced in core He burning but ^{64}Zn is destroyed in convective C shell; they are also produced in α -rich freeze-out layers in complete explosive Si-burning (LC03, WW95, Woosley et al. 2002, Nomoto et al. 2013). These contributions do not explain however, the high $[\text{Zn}/\text{Fe}]$ observed in metal-poor stars. Umeda & Nomoto (2002, 2005), Nomoto et al. (2013) suggested that ^{64}Zn is produced in energetic explosive nucleosynthesis so-called hypernovae.

Figure 13 shows $[\text{Zn}/\text{Fe}]$ vs. $[\text{Fe}/\text{H}]$ for the present sample, and bulge field stars from Barbuy et al. (2015), Bensby et al. (2013, 2017), and metal-poor stars from Howes et al. (2015, 2016), Casey & Schlafman (2016) and Koch et al. (2016), and for thick disk stars data from Ishigaki et al. (2013) and Nissen et al. (2011).

A high Zn abundance is found for bulge metal-poor stars in the range $-3.0 \lesssim [\text{Fe}/\text{H}] \lesssim -0.8$. This behaviour is similar to that previously reported in metal-poor halo and disk stars (e.g. Sneden et al. 1991; Nissen & Schuster 2011). In all samples $[\text{Zn}/\text{Fe}]$ decreases with increasing metallicity, reaching a solar value at $[\text{Fe}/\text{H}] > -0.4$.

The nucleosynthesis taking place in hypernovae is needed to reproduce this Zn enhancement in metal-poor stars, as proposed by Umeda & Nomoto (2005), and Nomoto et al. (2013, and references therein). The contribution in Zn by hypernovae in the chemical evolution models by Barbuy et al. (2015) proved to be needed to reproduce the data (see their Fig. 12). As for the present results $[\text{Zn}/\text{Fe}]$ is enhanced in the metal-poor clusters and decreases with metallicity, following the literature data.

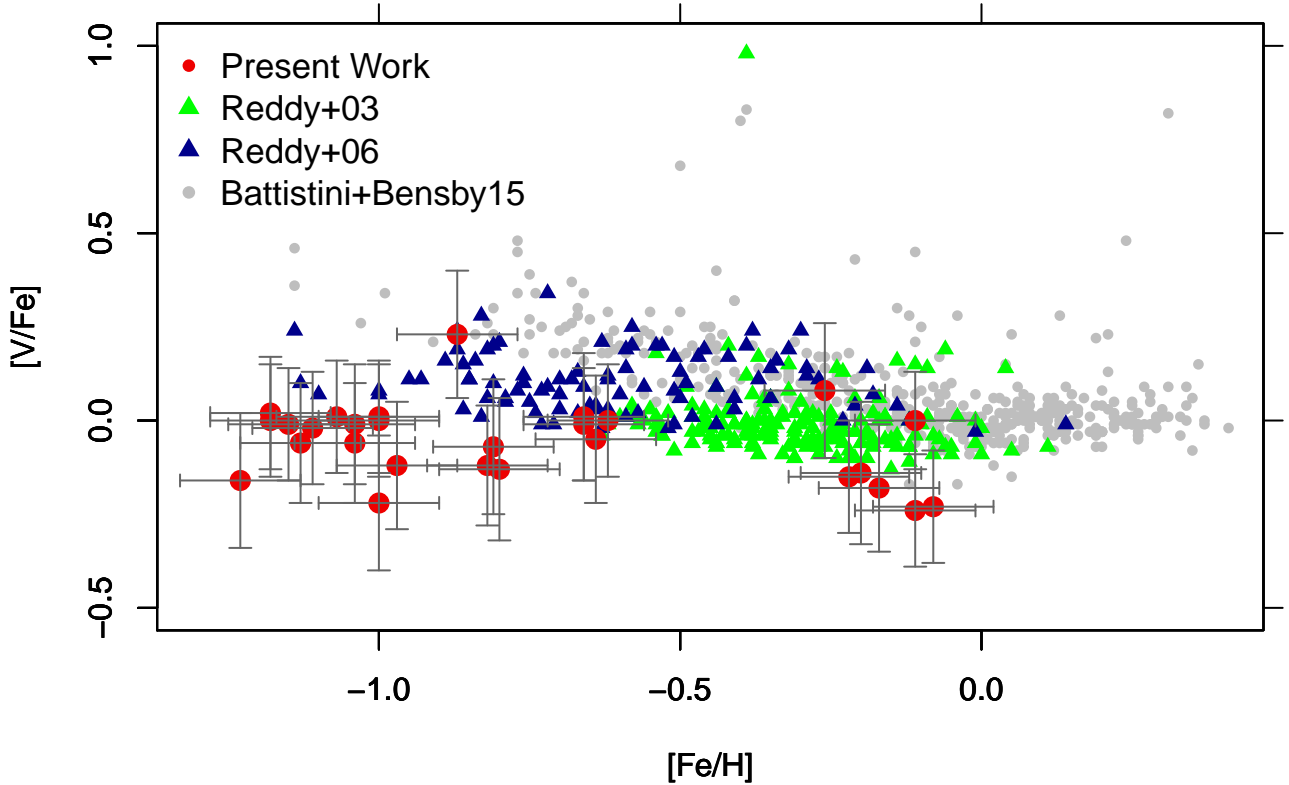


Fig. 8: $[V/Fe]$ vs. $[Fe/H]$. Symbols: present work (filled red circles); Reddy et al. (2003) (green filled triangles), Reddy et al. (2006) (navyblue filled triangles) Battistini & Bensby (2015) (grey filled circles). Errors are assumed as in Fig. 7.

The exception is the globular cluster HP 1, showing low $[Zn/Fe]$ at its metallicity of $[Fe/H] \sim -1.0$. A further inspection of this cluster would be of great interest, given that it has characteristics of being very old, and could reveal particularities due to its early formation.

Figure 13 compares $[Zn/Fe]$ vs. $[Fe/H]$ for bulge stars with chemodynamical evolution models of the Galactic bulge by Barbuy et al. (2015), further described in Friaça & Barbuy (2017). The hypernovae yields are suitable for metallicities more metal-poor than $[Fe/H] \lesssim -2.0$, as adopted in these models (Barbuy et al. 2015; Friaça & Barbuy 2017; da Silveira 2017). For this reason these models in the range $-2.0 < [Fe/H] < -1.0$ are interrupted. Models by Kobayashi et al. (2006) taking into account hypernovae also reproduce well the Zn behaviour.

For disk stars with $[Fe/H] > 0.0$, Reddy et al. (2003, 2006) obtained $[Zn/Fe] \sim 0.0$, Bensby et al. (2003, 2005) found $[Zn/Fe]$ essentially constant, whereas Allende-Prieto et al. (2004) found increasing $[Zn/Fe]$ with increasing metallicity.

The Bensby et al. (2013, 2017) results for microlensed dwarf bulge stars also give a solar $[Zn/Fe]$ at all metallic-

ities, differently from Barbuy et al. (2015), where $[Zn/Fe]$ decreases sharply at the high metallicity end. The present results for the metal-rich clusters also appear to decrease with increasing metallicity, despite some spread. This decrease implies the action of SNIa, and could be an evidence of differences in the chemical enrichment of bulge giants and a thick disk sample. It is interesting that Duffau et al. (2017) also found decreasing $[Zn/Fe]$ for red giants, and constant $[Zn/Fe]$ for dwarfs, at the supersolar metallicities. They interpreted this discrepancy in terms of stellar populations, i.e. that their red giants should be younger than the dwarfs, and for this reason, to contain Fe enriched from SNIa. The age explanation does not fit the present data, because our sample consists of old globular clusters. Stars in NGC 6528 have subsolar $[Zn/Fe]$, whereas NGC 6553 has $[Zn/Fe] \sim +0.3$ for one star, and subsolar in the other star. In particular, at its location in the Galaxy, NGC 6553 has kinematical characteristics compatible with bulge or disk stars (Zoccali et al. 2001b), whereas NGC 6528 is located in the bulge, so that they might be different from each other. In conclusion, there seems to be a trend to have decreasing Zn-to-Fe with increasing metallicity, despite it

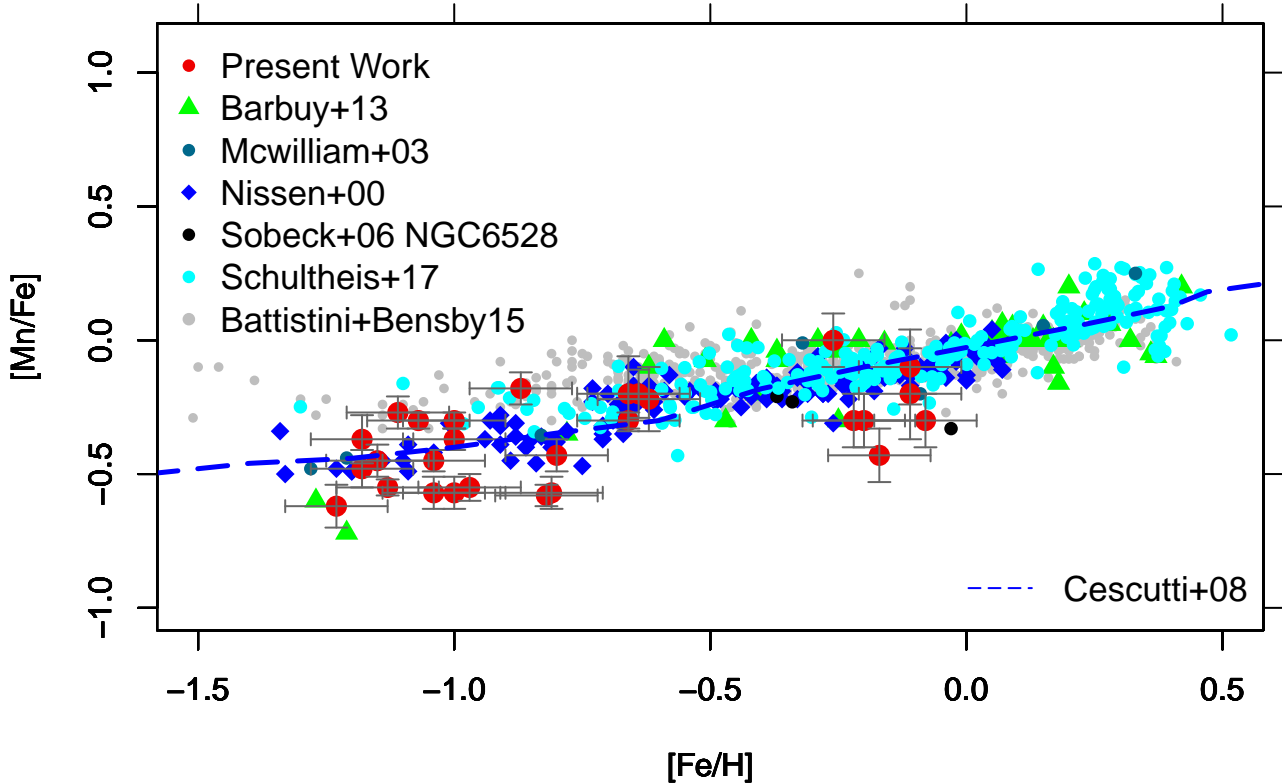


Fig. 9: $[\text{Mn}/\text{Fe}]$ vs. $[\text{Fe}/\text{H}]$ for the sample stars and literature data: the present sample (red filled circles), Nissen et al. (2000) (blue filled diamonds), Sobeck et al. (2006) (black filled circles), McWilliam et al. (2003) (deep sky blue filled circles), Barbuy et al. (2013) (green filled triangles), Schultheis et al. (2017) (blue filled circles), and Battistini & Bensby (2015) (grey filled circles). Chemical evolution models by Cescutti et al. (2008) (blue dashed line); are overplotted. Errors are assumed as in Fig. 7.

not being clear for NGC 6553. Another aspect is the suggestion by Grisoni et al. (2017) that the local metal-rich thick disk consists of stars having migrated from the inner regions of the Galaxy. Recio-Blanco et al. (2017) has also advanced a possibility of this population corresponding to a dwarf galaxy that previously merged with the Milky Way in the solar vicinity. A question that comes to mind is if it would be possible that the metal-rich bulge stars either by Barbuy et al. (2015), or those by Bensby et al. (2017) correspond to the alpha-enhanced thick disk by Grisoni et al. (2017), and for testing this it would be of interest to derive Zn abundances in these metal-rich thick disk stars.

Skúladóttir et al. (2017) derived Zn abundances in stars of the dwarf galaxy Sculptor. They also find $[\text{Zn}/\text{Fe}]$ decreasing with increasing metallicities, and verified that the same occurs with other dwarf galaxies studied in the literature such as Sagittarius, Sextans, Draco and Ursa Minor. The authors suggest that it is more naturally explained by the enrichment of Fe, and no Zn enrichment

from SNIa, therefore a behaviour similar to that of alpha-elements, although other less likely possibilities are discussed.

Finally, a general comment is that there is a trend for the cluster stars to be deficient relative to field bulge stars for Sc, V, and Zn. In particular at the metal-rich end, it could be attributed to noise in the spectra. For the metal-poor clusters, on the other hand, further inspection would be of great interest, because it could have an impact in the interpretation of enrichment of these globular clusters.

6. Summary

Globular clusters of the Galactic bulge should trace the formation process of the central parts of the Galaxy. They are also tracers of the older stellar populations in the bulge. Chemical tagging is a next big step for the understanding of the Milky Way formation. The iron-peak elements have been little studied so far, but their study should help understanding: a) nucleosynthesis of these el-

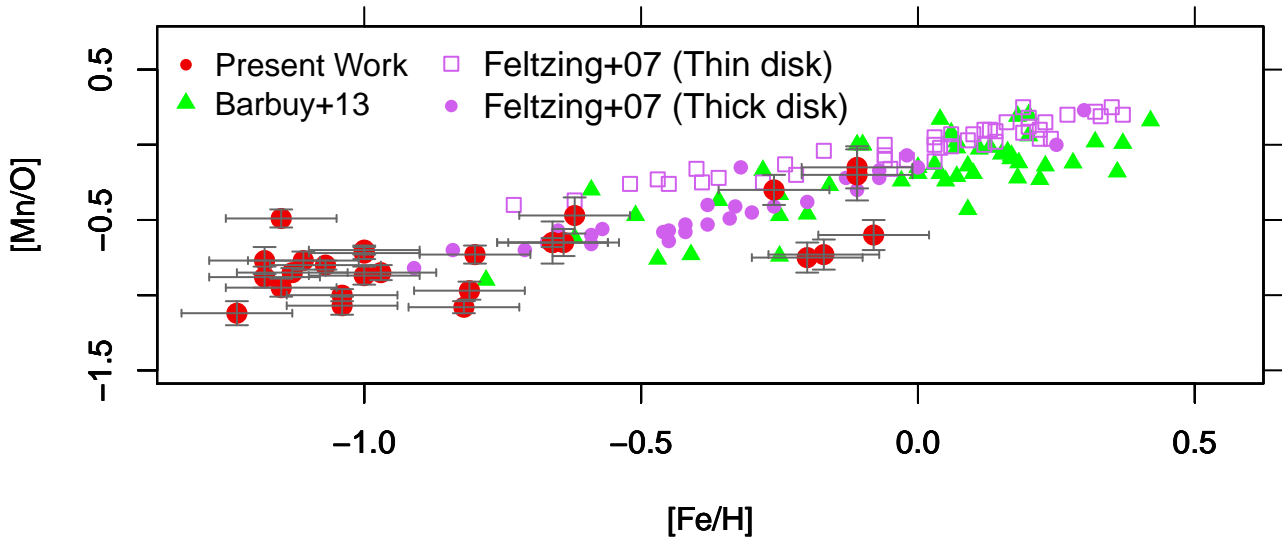


Fig. 10: $[\text{Mn}/\text{O}]$ vs. $[\text{Fe}/\text{H}]$. Symbols: present work (red filled circles), Barbuy et al. (2013) (green filled triangles), Feltzing et al. (2007) thin disk (violet open squares), Feltzing et al. (2007) thick disk (violet filled circles). Errors are assumed as in Fig. 7.

elements is complex and observations can help constraining their formation; b) Sc and V appear to vary in lockstep with Fe in the present sample, but Sc has been found to be alpha-like in thick disk and halo stars, and further studies are needed; c) Mn is deficient in metal-poor stars, and steadily increases with metallicity due to enrichment from SNIa; d) Cu shows a secondary-like behavior, in principle indicating its production in a weak s-process in massive stars; e) Zn is alpha-like in halo and thick disk stars, and also in the bulge, as concerns metal-poor stars. For metal-rich stars there is a controversy as to whether it decreases with increasing metallicity, or if $[\text{Zn}/\text{Fe}]$ keeps a solar value.

We have derived abundances of the iron-peak elements Sc, V, Mn, Cu, and Zn, in 23 red giants in the 5 bulge globular clusters NGC 6553, NGC 6528, HP 1, NGC 6522, NGC 6558, and 5 red giants in the reference inner halo/thick disk cluster 47 Tucanae. The work was based on FLAMES-UVES high-resolution spectra obtained at the VLT UT2 telescope.

Vanadium varies in lockstep with Fe. Sc behaves closely as V, not showing a clear enhancement, that was previously suggested by Nissen et al. (2000) for alpha-rich halo and thick disk stars. Both $[\text{Sc}, \text{V}/\text{Fe}]$ seem to decrease with increasing metallicity at the high metallicity end.

Mn is deficient in metal-poor stars and increases to solar values for the more metal-rich stars, indicating that it is underproduced in massive stars, and later produced in SNIa.

Cu show a behaviour as secondary elements, having low values at low metallicities, and steadily increasing with increasing metallicity, indicating an enrichment through a weak-s process in massive stars, and in good agreement with chemical evolution models.

Zn is enhanced in metal-poor stars, likewise an alpha-element, and decreases with increasing metallicity. At the high metallicity end the behaviour of the present data is different from that found by Bensby et al. (2013, 2017), that show solar ratios at the high metallicities. This could be a discriminator of having the contribution of SNIa or not. This is made less clear given the difference in $[\text{Zn}/\text{Fe}]$ found by Duffau et al. (2017) for red giants and dwarfs. Skúladóttir et al. (2017) found $[\text{Zn}/\text{Fe}]$ decreasing with metallicity for the dwarf galaxy Sculptor, and point out that the same is true for other dwarf galaxies. It is of great interest to pursue abundance derivation of iron-peak elements, and in particular Sc in all stellar populations, and Zn in bulge stars.

Acknowledgements. We acknowledge grants and fellowships from FAPESP, CNPq and CAPES.

References

- Alonso, A., Arribas, S., Martínez-Roger, C. 1999, *A&AS*, 140, 261
- Allende Prieto, C., Lambert, D.L., Asplund, M. 2001, *ApJ*, 556, L63
- Alves-Brito, A., Barbuy, B., Ortolani, S., Momany, Y., Hill, V., Zoccali, M., Renzini, A., Minniti, D., Pasquini, L., Bica, E. & Rich, R.M. 2005, *A&A*, 435, 657

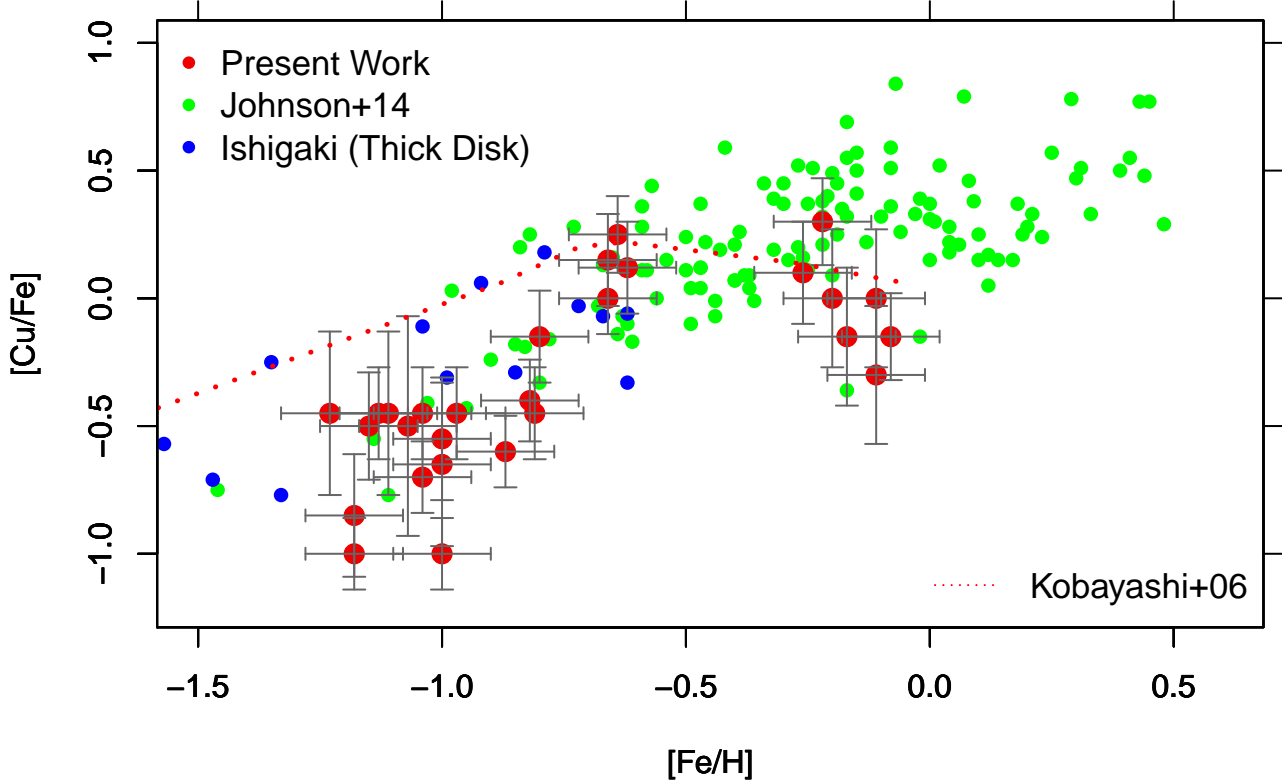


Fig. 11: $[\text{Cu}/\text{Fe}]$ vs. $[\text{Fe}/\text{H}]$ for the present sample (red filled circles), Johnson et al. (2014) (green filled circles), and Ishigaki et al. (2013) (blue filled circles). Chemical evolution models by and Kobayashi et al. (2006) (red dotted lines) are overplotted. Errors are assumed as in Fig. 7.

- Alves-Brito, A., Barbuy, B., Zoccali, M., Minniti, D., Ortolani, S., Hill, V., Renzini, A., Pasquini, L., Bica, E., Rich, R.M. & Meléndez, J. *A&A*, 2006, 460, 269.
- Asplund, M., Grevesse, N., Sauval, A.J., Scott, P. 2009, *ARA&A*, 47, 481
- Ballester, P., Modigliani, A., Boitquin, O., Cristiani, S., Hanuschik, R., Kaufer, A., Wolf, S. 2000, in *The Messenger*, 101, 31.
- Barbuy, B., Bica, E., Ortolani, S. 1998, *A&A*, 333, 117
- Barbuy, B., Perrin, M.-N., Katz, D., Coelho, P., Cayrel, R., Spite, M., van't Veer-Menneret, C. 2003, *A&A*, 404, 661
- Barbuy, B., Zoccali, M., Ortolani, S., et al. 2006, *A&A*, 449, 349
- Barbuy, B., Zoccali, M., Ortolani, S., et al. 2009, *A&A*, 507, 405
- Barbuy, B., Chiappini, C., Cantelli, E. et al. 2014, *A&A*, 570, A76
- Barbuy, B., Hill, V., Zoccali, M., et al. 2013, *A&A*, 559, A5
- Barbuy, B., Chiappini, C., Cantelli, E., et al. 2014, *A&A*, 570, A76
- Barbuy, B., Friaça, A., da Silveira, C.R., et al. 2015, *A&A*, 580, A40
- Barbuy, B., Cantelli, E., Vemado, A., et al. 2016, *A&A*, 591, A53
- Barbuy, B., Siqueira-Mello, C., Muniz, L.I., et al. 2017, *A&A*, in preparation
- Barbuy, B., Chiappini, C., Gerhard, O. 2018, *ARA&A*, in press
- Battistini, C., Bensby, T., 2015, *A&A*, 577, A9
- Bensby, T., Feltzing, S., Lundström, I., 2003, *A&A*, 410, 527
- Bensby, T., Feltzing, S., Lundström, I., Ilyin, I. 2005, *A&A*, 433, 185
- Bensby, T., Yee, J.C., Feltzing, S. et al. 2013, *A&A*, 549, A147
- Bensby, T., Feltzing, S., Gould, A., et al. 2017, *A&A*, **605**, A89
- Bergemann, M., Gehren, T. 2008, *A&A*, 492, 823
- Biehl, H. 1976, University of Kiel
- Bielski, A. 1975, *JQSRT*, 15, 463
- Casey, A.R., Schlaufman, K.C. 2015, *ApJ*, 809, 110
- Cayrel, R. 1988, in *IAU Symposium, Vol. 132, The Impact of Very High S/N Spectroscopy on Stellar Physics*, ed. G. Cayrel de Strobel & M. Spite, 345
- Cayrel, R., Depagne, E., Spite, M., Hill, V., Spite, F. et al. 2004, *A&A*, 416, 1117
- Cescutti, G., Matteucci, F., Lanfranchi, G. 2008, *A&A*, 491, 401
- Coelho, P., Barbuy, B., Meléndez, J., Schiavon, R.P., Castilho, B.V. 2005, *A&A*, 443, 735
- da Silveira, C.R. 2017, PhD thesis, Universidade de São Paulo

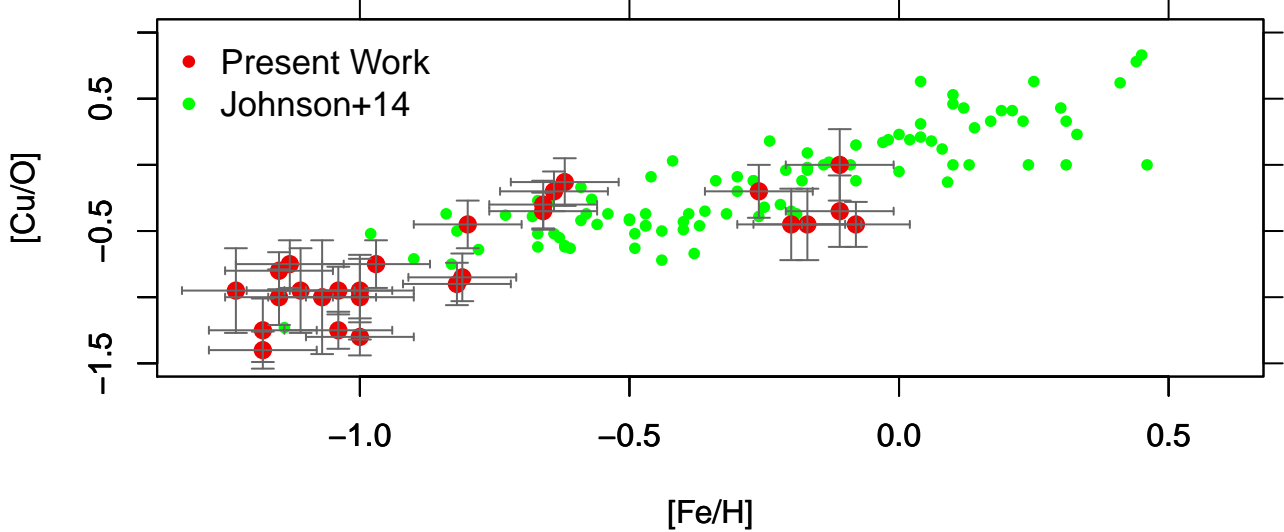


Fig. 12: $[Cu/O]$ vs. $[Fe/H]$. Symbols: present work (red filled circles), and Johnson et al. (2014) (green filled circles).

- Duffau, S., Caffau, E., Sbordone, L. et al. 2017, *A&A*, **605**, **A128**
- Feltzing, S., Fohlman, M., Bensby, T. 2007, *A&A*, 467, 665
- Fishlock, C.K., Yong, D., Karakas, A.I. et al. 2017, *MNRAS*, 466, 4672
- Freeman K, Bland-Hawthorn J. 2002, *ARA&A*, 40, 487
- Friaca A.C.S., Barbuy B. 2017. *A&A*, 598, 121
- Fulbright, J.P., McWilliam, A., Rich, R.M. 2007, *ApJ*, 661, 1152
- Gratton, R.G., Sneden, C. 1990, *A&A*, 234, 366
- Gratton, R.G., Carretta, E., Bragaglia, A. 2012, *A&ARv*, 20, 50
- Grevesse, N., Noels, A., Sauval, J. 1996, *ASP Series*, 99, 117
- Grevesse, N., Noels, A. & Sauval, J.N. 1996, *ASPC*, 99, 117
- Grisoni, V., Spitoni, E., Matteucci, F. et al. 2017, *MNRAS*, 472, 3637
- Guarnieri, M.D., Ortolani, S., Montegriffo, P., et al. 1998, *A&A*, 331, 70
- Gustafsson, B., Edvardsson, B., Eriksson, K. et al. 2008, *A&A*, 486, 951
- Harris W. 1996, *AJ*, 112, 1487
- Hansen, B.M.S., Kalirai, J.S., Anderson, J. et al. 2013, *Nature*, 500, 51
- Hinkle, K., Wallace, L., Valenti, J., Harmer, D. 2000, *Visible and Near Infrared Atlas of the Arcturus Spectrum 3727-9300 A*, ed. K. Hinkle, L. Wallace, J. Valenti, and D. Harmer (San Francisco: ASP)
- Houdashelt, M.L., Bell, R.A., Sweigart, A.V. 2000, *AJ*, 119, 1448
- Howes, L.M., Asplund, M., Casey, A.R., Keller, S.C., Yong, D., et al. 2014, *MNRAS*, 445, 4241
- Howes, L.M., Casey, A.R., Asplund, M., Keller, S.C., Yong, D., et al. 2015, *Nature*, 527, 484
- Howes, L.M., Asplund, M., Keller, S.C., Casey, A.R., Yong, D., et al. 2016, *MNRAS*, 460, 884
- Ishigaki, M.N., Aoki, W., Chiba, M. 2013, *ApJ*, 771, 67
- Iwamoto, K., Brachwitz, F., Nomoto, K., Kishimoto, N., Umeda, H., Hix, W. R., Thielemann, F. 1999, *ApJS*, 125, 439
- Johnson, C.I., Rich, R.M., Kobayashi, C., Kunder, A., Koch, A. 2014, *AJ*, 148, 67
- Kobayahi, C., Umeda, H., Nomoto, K., Tominaga, N., Ohkubo, T. 2006, *ApJ*, 653, 1145
- Koch, A., McWilliam, A., Preston, G.W., Thompson, I.B. 2016, *A&A*, 587, 124
- Kraft, R.P. 1983, in *Highlights of Astronomy*, 6, 129
- Kruijssen, J.M.D. 2015, *MNRAS*, 454, 1658
- Kurucz, R. 1993, *CD-ROM* 23
- Lecureur, A., Hill, V., Zoccali, M., Barbuy, B., Gómez, A., et al. 2007, *A&A*, 465, 799
- Limongi, M., Chieffi, A. 2003. *ApJ*, 592, 404
- Martell, S.L., Smolinski, J.P., Beers, T.C., Grebel, E.K. 2011, *A&A*, 534, A136
- Martin, W.C., Fuhr, J.R., Kelleher, D.E., et al. 2002, *NIST Atomic Database (version 2.0)*, <http://physics.nist.gov/asd>. National Institute of Standards and Technology, Gaithersburg, MD.
- McWilliam, A. 2016, *PASA*, 33, 40
- McWilliam, A., Rich, R. M., Smecker-Hane, T. A. 2003, *ApJ*, 592, L21
- McWilliam, A., Wallerstein, G., Mottini, M. 2013, *ApJ*, 778, 149
- Meléndez, J., Barbuy, B., Bica, E. et al. 2003, *A&A*, 411, 417
- Nissen, P.E., Chen, Y.Q., Schuster, W.J., Zhao, G. 2000, *A&A*, 353, 722
- Nissen, P.E., Schuster, W.J., 2011, *A&A*, 530, 15
- Nomoto, K., Kobayashi, C., Tominaga, N. 2013, *ARA&A*, 51, 457
- Ortolani, S., Barbuy, B., Bica, E., Zoccali, M., Renzini, A. 2007, *A&A*, 470, 1043

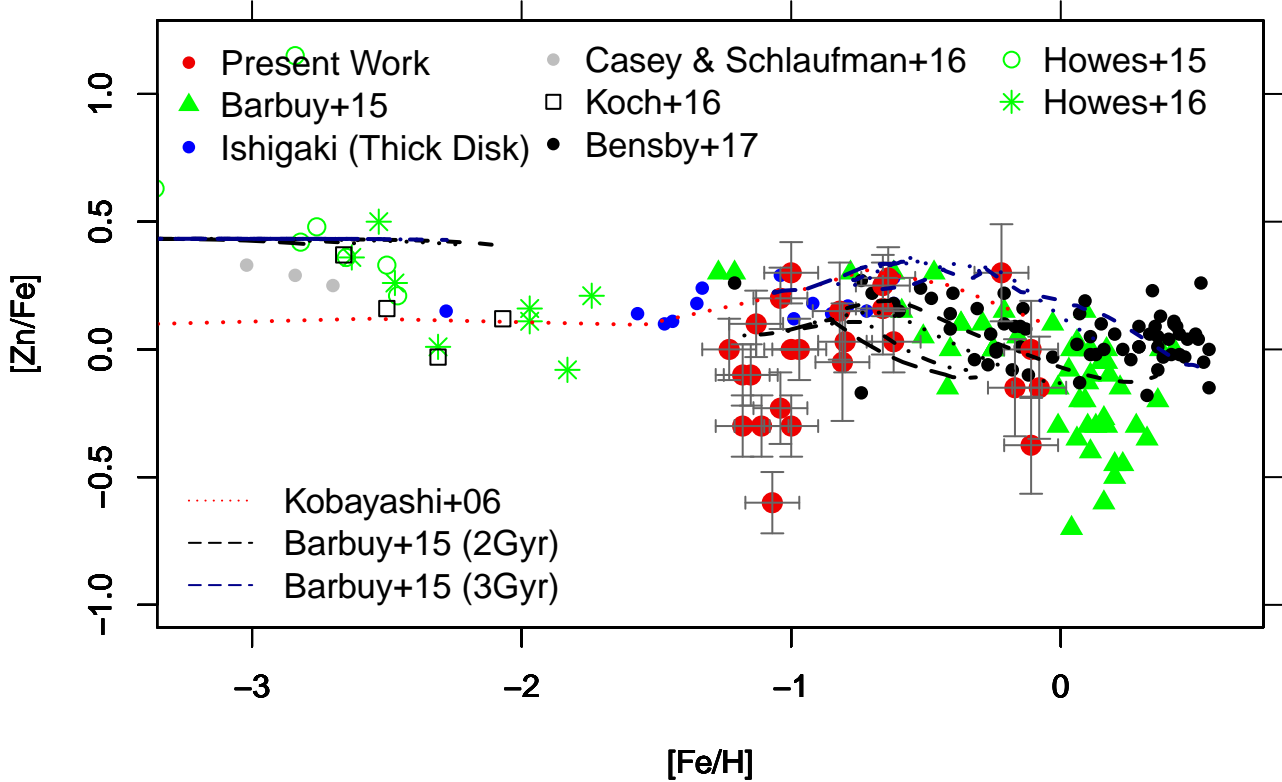


Fig. 13: $[Zn/Fe]$ vs. $[Fe/H]$. Symbols: present work (filled red circles), Barbuy et al. (2015) (green filled triangles), Ishigaki et al. (2013) (blue filled circles), Howes et al. (2015) (green open circles), Howes et al. (2016) (green crosses), Casey & Schlafman (2016) (grey filled circles), Koch et al. (2016) (black open squares), Bensby et al. (2017) (black filled circles). Chemical evolution models by Kobayashi et al. (2006) (red dotted line). The Barbuy et al. (2015) models are shown for enrichment timescales of 2 (black) and 3 (blue) Gyr. In each case, the models for radius with respect to the Galactic center of $r < 0.5$ kpc (dashed lines), $0.5 < r < 1$ kpc (dotted lines), $1 < r < 2$ kpc (dashe-dotted lines), $2 < r < 3$ kpc (long-dashed lines) are overplotted. Errors are assumed as in Fig. 7.

- Ortolani, S., Barbuy, B., Momany, Y., Saviane, I., Bica, E. et al. 2011, *ApJ*, 737, 31
- Pignatari, M., Gallino, R., Heil, M., Wiescher, M., Kppeler, F., Herwig, F., Bisterzo, S. 2010, *ApJ*, 710, 1557P
- Piskunov, N., Kupka, F., Ryabchikova, T., Weiss, W., Jeffery, C., 1995, *A&AS*, 112, 525
- Pompéia, L., Hill, V., Spite, M. et al. 2008, *A&A*, 480, 379
- Ramírez, I., Allende-Prieto, C. 2011, *ApJ*, 743, 135
- Recio-Blanco, A. et al. 2017, *IAU Symposium 334*, in press
- Reddy, B.E., Tomkin, J., Lambert, D.L., Allende Prieto, C. 2003, *MNRAS*, 340, 304
- Reddy, B.E., Lambert, D.L., Allende Prieto, C. 2006, *MNRAS*, 367, 1329
- Renzini, A. 2017, *MNRAS*, 469, L63
- Rossi, L., Ortolani, S., Barbuy, B., Bica, E., Bonfanti, A. 2015, *MNRAS*, 450, 3270
- Schiavon, R.P., Zamora, O., Carrera, R., et al. 2017, *MNRAS*, 465, 501
- Schultheis, M., Rojas-Arriagada, A., García-Pérez, A.E., Jönsson, H., Hayden, M., et al. 2017, *A&A*, 600, A14
- Skúladóttir, Á., Tolstoy, E., Salvadori, S., Hill, V., Pettini, M. 2017, *A&A*, in press
- Smith, V.V., Cunha, K., Shetrone, M.D. et al. 2013, *ApJ*, 765, 16
- Snedden, C., Gratton, R. G., Crocker, D. A. 1991, *A&A*, 246, 354S
- Sobeck, J.S., Ivans, I. I., Simmerer, J. A., Sneden, C., Hoeflich, P., Fulbright, J. P., Kraft, R. P., 2006, *AJ*, 131, 2949
- Steffen, M., Prakashavicius, D., Caffau, E. et al. 2015, *A&A*, 583, A57
- Terndrup, D.M. 1988, *AJ*, 96, 884
- Umeda, H., Nomoto, K., 2002, *ApJ*, 565, 385
- Umeda, H., Nomoto, K., 2003, *Nature*, 422, 871
- Umeda, H., Nomoto, K., 2005, *ApJ*, 619, 427
- Woolsey, S. E., Weaver, T. A. 1995, *ApJS*, 101, 181
- Woolsey, S., Heger, A., Weaver, T.A. 2002. *Rev. Mod. Phys.* 74, 1015
- Zoccali, M., Renzini, A., Ortolani, S., Bragaglia, A., Böhlín, R. et al. 2001a, *ApJ*, 553, 733
- Zoccali, M., Renzini, A., Ortolani, S., Bica, E., Barbuy, B. 2001b, *AJ*, 121, 2638

Table 6: Line-by-line abundance ratios of Sc, V, Mn, Cu, Zn for the sample.

		47 Tucanae					NGC 6553				NGC 6528			HP 1	
Line	$\lambda(\text{\AA})$	M8	M11	M12	M21	M25	II-64	II-85	III-8	267092	I-18	I-36	I-42	2	3
ScI	5671.805	+ 0.00	+ 0.03	+ 0.05	+ 0.00	-0.10	-0.30	-0.30	-0.30	-0.15	-0.30	-0.30	+ 0.00	—	+ 0.00
ScI	5686.826	+ 0.00	+ 0.00	+ 0.10	—	+ 0.00	-0.30	+ 0.00	-0.30	-0.25	-0.30	-0.50	+ 0.00	+ 0.00	—
ScI	6210.676	-0.25	-0.30	-0.10	—	-0.20	-0.30	—	-0.30	-0.30	-0.50	-0.60	-0.30	+ 0.00	+ 0.00
ScII	5526.790	+ 0.00	-0.30	+ 0.05	+ 0.00	+ 0.00	-0.30	+ 0.00	-0.30	+ 0.00	-0.40	-0.30	-0.30	-0.15	+ 0.00
ScII	5552.224	+ 0.00	+ 0.00	—	—	+ 0.10	+ 0.00	+ 0.30	+ 0.00	—	—	—	—	—	+ 0.00
ScII	5657.896	+ 0.20	+ 0.15	+ 0.30	+ 0.00	+ 0.30	+ 0.00	+ 0.30	+ 0.00	+ 0.30	-0.30	+ 0.00	+ 0.00	+ 0.00	+ 0.00
ScII	5684.202	+ 0.30	+ 0.05	+ 0.30	+ 0.00	+ 0.30	-0.10	+ 0.30	-0.25	+ 0.00	-0.30	-0.30	+ 0.00	+ 0.00	+ 0.00
ScII	6245.637	+ 0.10	+ 0.00	+ 0.00	+ 0.00	+ 0.25	+ 0.00	+ 0.10	-0.30	+ 0.00	-0.30	-0.30	—	+ 0.00	+ 0.00
ScII	6300.698	+ 0.15	+ 0.00	+ 0.10	—	+ 0.00	+ 0.00	+ 0.25	-0.15	—	-0.30	-0.40	+ 0.00	+ 0.00	+ 0.30
ScII	6320.851	+ 0.15	+ 0.10	+ 0.25	+ 0.00	+ 0.20	+ 0.00	—	+ 0.00	+ 0.00	-0.30	-0.30	+ 0.00	+ 0.00	+ 0.00
ScII	6604.601	+ 0.15	+ 0.00	+ 0.05	-0.10	+ 0.00	-0.15	—	-0.30	+ 0.00	-0.35	-0.45	-0.30	-0.20	-0.15
VI	5703.560	+ 0.10	+ 0.00	+ 0.10	-0.20	+ 0.00	+ 0.00	+ 0.25	-0.25	+ 0.00	-0.12	-0.10	+ 0.00	-0.30	+ 0.00
VI	6081.440	-0.10	+ 0.00	-0.05	-0.30	-0.10	-0.10	—	-0.10	-0.15	-0.30	-0.15	+ 0.00	-0.30	-0.25
VI	6090.220	+ 0.00	+ 0.00	+ 0.15	-0.05	+ 0.00	-0.25	+ 0.00	-0.15	-0.15	-0.25	-0.30	+ 0.00	-0.30	-0.10
VI	6119.520	+ 0.00	+ 0.05	+ 0.12	-0.05	+ 0.00	+ 0.00	+ 0.00	+ 0.00	-0.15	-0.10	-0.30	+ 0.00	—	-0.20
VI	6199.190	-0.15	+ 0.00	-0.10	-0.10	+ 0.00	-0.30	—	-0.10	-0.30	-0.30	-0.30	+ 0.00	-0.10	-0.12
VI	6243.100	-0.10	+ 0.00	+ 0.00	+ 0.00	+ 0.00	-0.35	—	-0.25	-0.15	-0.20	-0.30	+ 0.00	-0.15	-0.10
VI	6251.820	-0.10	+ 0.00	+ 0.00	-0.30	+ 0.00	+ 0.00	—	-0.30	-0.15	-0.30	-0.30	+ 0.00	-0.30	-0.05
VI	6274.650	-0.10	+ 0.00	-0.10	-0.15	+ 0.00	-0.15	—	-0.30	-0.15	-0.20	-0.15	+ 0.00	-0.10	—
VI	6285.160	+ 0.00	-0.05	+ 0.00	+ 0.00	+ 0.00	—	—	—	—	-0.30	—	—	—	—
MnI	6013.513	-0.10	-0.05	+ 0.00	-0.40	-0.30	-0.30	+ 0.00	-0.45	-0.30	-0.30	+ 0.00	+ 0.00	-0.60	-0.50
MnI	6016.640	-0.30	-0.30	-0.30	-0.40	-0.30	-0.30	—	-0.45	-0.30	-0.30	-0.30	—	-0.60	-0.55
MnI	6021.800	-0.20	-0.30	-0.30	-0.50	-0.30	-0.30	+ 0.00	-0.40	—	-0.30	-0.30	-0.20	-0.50	-0.60
CuI	5105.537	+ 0.20	+ 0.00	+ 0.00	-0.30	+ 0.00	-0.30	-0.10	-0.30	+ 0.00	-0.30	-0.30	-0.60	—	-0.60
CuI	5218.197	+ 0.30	+ 0.30	+ 0.30	+ 0.00	+ 0.00	—	—	-0.15	+ 0.30	-0.15	-0.45	—	-1.00	-0.30
ZnI	4810.529	+ 0.25	+ 0.00	+ 0.02	+ 0.05	+ 0.25	—	—	-0.05	+ 0.30	+ 0.00	-0.30	—	—	+ 0.00
ZnI	6362.339	+ 0.30	+ 0.05	+ 0.30	+ 0.05	+ 0.25	—	—	-0.00	+ 0.30	+ 0.00	-0.30	—	—	+ 0.00

		HP-1					NGC 6522			NGC 6558					
Line	$\lambda(\text{\AA})$	2115	2461	2939	3514	5037	5485	B-107	B-122	B-128	B-130	283	364	1072	1160
ScI	5671.805	-0.10	—	+0.12	+0.05	-0.12	—	—	+0.00	-0.30	—	—	—	—	—
ScI	5686.826	+0.10	—	+0.25	—	—	—	—	—	—	—	—	—	—	—
ScI	6210.676	+0.15	—	+0.15	—	-0.05	—	—	—	-0.05	—	—	—	—	—
ScII	5526.790	-0.15	+0.00	+0.00	-0.30	-0.18	-0.30	+0.00	+0.00	+0.00	-0.05	-0.30	-0.15	-0.15	-0.15
ScII	5552.224	+0.30	—	—	—	—	—	-0.30	—	—	+0.30	—	—	—	—
ScII	5657.896	+0.00	+0.00	+0.30	+0.00	+0.10	+0.15	+0.00	+0.05	+0.00	+0.00	-0.3	-0.15	+0.30	-0.10
ScII	5684.202	+0.00	+0.00	+0.00	-0.15	+0.00	+0.00	-0.15	+0.10	+0.00	+0.00	+0.00	-0.10	+0.30	—
ScII	6245.637	+0.10	+0.00	+0.30	+0.00	+0.12	+0.03	-0.10	+0.15	+0.00	+0.00	-0.03	—	-0.30	-0.20
ScII	6300.698	+0.30	+0.00	—	+0.30	+0.30	—	—	+0.00	+0.00	+0.00	—	+0.60	—	+0.00
ScII	6320.851	+0.00	+0.15	+0.30	+0.30	+0.15	+0.00	-0.15	+0.15	+0.30	+0.15	+0.00	—	+0.15	-0.30
ScII	6604.601	+0.00	+0.00	+0.30	+0.30	+0.00	-0.05	-0.30	+0.05	+0.15	+0.00	+0.00	—	+0.10	-0.05
VI	5703.560	+0.00	-0.10	+0.00	+0.00	+0.00	+0.00	—	-0.20	-0.10	-0.05	-0.05	+0.00	-0.30	+0.00
VI	6081.440	+0.00	—	+0.00	+0.02	+0.00	+0.00	—	-0.25	-0.10	-0.15	+0.05	+0.30	+0.00	+0.00
VI	6090.220	+0.00	+0.00	+0.00	+0.00	+0.00	—	+0.00	+0.00	-0.15	-0.1	-0.05	+0.00	-0.15	-0.10
VI	6119.520	+0.05	+0.00	+0.00	+0.00	+0.00	—	+0.00	+0.00	-0.15	+0.0	-0.05	+0.00	+0.00	-0.10
VI	6199.190	+0.00	-0.05	+0.00	+0.05	+0.00	—	—	+0.00	+0.00	+0.0	+0.00	—	-0.30	+0.05
VI	6243.100	+0.00	+0.00	+0.00	+0.05	+0.00	+0.00	-0.15	+0.00	-0.10	+0.0	+0.00	—	-0.20	+0.00
VI	6251.820	+0.00	+0.00	+0.05	+0.00	+0.00	+0.00	—	-0.10	+0.0	-0.05	+0.00	+0.15	-0.15	+0.10
VI	6274.650	—	+0.00	+0.00	+0.00	+0.00	—	-0.10	+0.00	-0.25	-0.15	—	—	-0.15	+0.00
VI	6285.160	—	—	—	—	—	—	—	—	—	—	—	—	—	—
MnI	6013.513	-0.30	-0.3	-0.30	-0.30	-0.35	-0.40	-0.55	-0.50	-0.55	-0.50	-0.50	-0.25	-0.60	-0.50
MnI	6016.640	-0.30	-0.3	-0.30	-0.30	-0.35	-0.55	-0.55	-0.60	-0.60	-0.60	—	-0.32	-0.60	-0.35
MnI	6021.800	-0.30	-0.2	-0.30	-0.50	-0.40	-0.50	-0.55	-0.60	-0.60	-0.60	-0.40	-0.30	-0.65	-0.50
CuI	5105.537	-0.80	-0.8	-1.00	-1.10	-1.00	-1.00	-0.60	-0.60	-0.50	-0.60	-0.70	-0.60	-0.80	-0.70
CuI	5218.197	-0.30	-0.1	+0.00	-0.60	-0.30	—	-0.30	-0.30	-0.30	-0.30	-0.30	—	-0.1	—
ZnI	4810.529	—	-0.30	-0.60	-0.10	-0.30	-0.30	+0.05	-0.25	+0.00	-0.30	-0.10	—	+0.00	+0.20
ZnI	6362.339	—	—	—	—	—	—	+0.15	+0.15	+0.30	- 0.15	—	—	—	—

Zoccali, M., Barbuy, B., Hill, V., Ortolani, S., Renzini, A., Bica, E., Momany, Y., Pasquini, L., Minniti, D., & Rich, R.M. 2004, A&A, 423, 507
Zoccali, M., Lecureur, A., Barbuy, B., Hill, V., Renzini, A., et al. 2006, A&A, 457, L1
Zoccali, M., Hill, V., Lecureur, A., Barbuy, B., Renzini, A., et al. 2008, A&A, 486, 177

Appendix A: Atomic data

In Table A.1 are given the hyperfine structure constants of Sc, V and Cu lines.

Table 7: Mean abundances of Sc, V, Mn, Cu, Zn for the sample.

Stars	Mean abundances												
	[Fe/H]	[ScI/Fe]	$\delta_{[ScI/Fe]}$	[ScII/Fe]	$\delta_{[ScII/Fe]}$	[VI/Fe]	$\delta_{[VI/Fe]}$	[MnI/Fe]	$\delta_{[MnI/Fe]}$	[CuI/Fe]	$\delta_{[CuI/Fe]}$	[ZnI/Fe]	$\delta_{[ZnI/Fe]}$
47Tuc													
M8	-0.64	-0.08	0.12	+0.13	0.08	-0.05	0.07	-0.20	0.08	+0.25	0.04	+0.28	0.03
M11	-0.62	-0.09	0.15	+0.04	0.06	+0.00	0.02	-0.22	0.12	+0.12	0.12	+0.03	0.03
M12	-0.66	+0.02	0.08	+0.15	0.12	+0.01	0.09	-0.20	0.14	+0.15	0.12	+0.16	0.14
M21	-0.80	+0.00	0.08	-0.02	0.04	-0.13	0.11	-0.43	0.05	-0.15	0.12	+0.03	0.03
M25	-0.66	-0.10	?	+0.14	0.12	-0.01	0.03	-0.30	0.00	+0.00	0.00	+0.25	0.00
NGC 6553													
II-64	-0.20	-0.30	0.00	-0.06	0.06	-0.14	0.13	-0.30	0.00	+0.00	0.24	—	—
II-85	-0.26	-0.15	0.15	+0.21	0.08	+0.08	0.12	+0.00	0.00	+0.10	0.16	—	—
III-8	-0.17	-0.30	0.00	-0.16	0.13	-0.18	0.10	-0.43	0.02	+0.15	0.24	-0.15	0.03
III-9	-0.22	-0.23	0.06	+0.05	0.12	-0.15	0.08	-0.30	0.00	+0.30	0.12	+0.30	0.00
NGC 6528													
I-18	-0.08	-0.37	0.09	-0.32	0.02	-0.23	0.08	-0.30	0.00	-0.15	0.12	-0.15	0.08
I-36	-0.11	-0.47	0.12	-0.29	0.14	-0.24	0.08	-0.20	0.14	+0.00	0.24	-0.37	0.03
I-42	-0.11	-0.10	0.14	-0.10	0.12	+0.00	0.00	-0.10	0.10	-0.30	0.24	—	?
HP 1													
2	-1.00	+0.00	?	-0.05	0.07	-0.22	0.09	-0.57	0.05	-1.00	?	+0.30	?
3	-0.97	+0.00	?	-0.02	0.12	-0.12	0.08	-0.55	0.04	-0.45	0.12	+0.00	?
2115	-1.00	+0.05	0.11	+0.07	0.13	+0.01	0.02	-0.30	0.00	-0.55	0.20	—	—
2461	-1.11	—	—	+0.02	0.06	-0.02	0.04	-0.27	0.05	-0.45	0.29	-0.30	?
2939	-1.07	+0.17	0.06	+0.20	0.12	+0.01	0.02	-0.30	0.00	-0.50	0.41	-0.60	?
3514	-1.18	+0.05	?	+0.06	0.18	+0.02	0.02	-0.37	0.09	-0.85	0.20	-0.10	?
5037	-1.00	-0.09	0.04	+0.08	0.10	+0.00	0.00	-0.37	0.02	-0.65	0.29	-0.30	?
5485	-1.18	—	—	-0.03	0.07	+0.00	0.00	-0.48	0.06	-1.00	?	-0.30	?
NGC 6522													
B-107	-1.13	—	—	-0.11	0.12	-0.06	0.06	-0.55	0.00	-0.45	0.12	+0.10	0.05
B-122	-0.81	+0.00	?	+0.07	0.06	-0.07	0.10	-0.57	0.05	-0.45	0.12	-0.05	0.20
B-128	-0.82	-0.18	0.13	+0.06	0.11	-0.12	0.07	-0.58	0.02	-0.40	0.08	+0.15	0.15
B-130	-1.04	—	—	+0.05	0.11	-0.06	0.06	-0.57	0.05	-0.45	0.12	-0.23	0.08
NGC6558													
283	-1.15	—	—	-0.16	0.16	-0.01	0.03	-0.45	0.05	-0.50	0.16	-0.10	?
364	-1.15	—	—	+0.05	0.32	+0.09	0.12	-0.29	0.03	-0.60	?	—	—
1072	-1.23	—	—	+0.07	0.22	-0.16	0.11	-0.62	0.07	-0.45	0.29	+0.00	?
1160	-1.04	—	—	-0.13	0.11	-0.01	0.06	-0.45	0.02	-0.70	?	+0.20	?

Table A.1: Atomic constants for ScI and ScII used to compute hyperfine structure: A and B constants from Mansour, N. B., Dinneen, T. P., Young, L. 1989, NIMPB, 40-252M, Villemoes et al. 1992, PhRvA, 45-6241V for ScII and Biehl (1976) for ScI. For VI the A and B constants are from 1 UBDE Unkel, P., Buch, P., Dembczynski, J., Ertmer, W., and Johan, U. 1989, Z. Phys. D 11, 259-271. 2 CPGC Childs, W.J., Poulsen, O., Goodman, L.S., and Crosswhite, H. 1979, Phys. Rev. A 19, 168-176. 3 PBAG Palmeri, P., Biemont, E., Aboussaid, A., and Godefroid, M. 1995, J.Phys.B 28, 3741-3752. 4 CFBG Cochrane, E.C.A., Benton, D.M., Foreset, D.H., and Griffith, J.A.R. 1998, J.Phys.B 31, 2203-2213. 5 LGB Lefebvre, P-H, Garnir, H-P, Biemont, E 2002, Physica Scripta 66, 363-366. B constants not available in the literature are assumed as null.

species	λ (Å)	Lower level	J	A(mK)	A(MHz)	B(mK)	B(MHz)	Upper level	J	A(mK)	A(MHz)	B(mK)	B(MHz)
⁴⁵ ScI	5671.805	3d ² (³ F)4s 4F	9/2	+9.5	284.8029	-0.4	-11.9917	3d ² (³ F)4p ⁴ G	11/2	+1.5	44.9689	—	—
⁴⁵ ScI	5686.826	3d ² (³ F)4s 4F	7/2	+8.3	248.8278	-0.3	-8.9938	3d ² (³ F)4p 4G	7/2	+4.9	146.8983	—	—
⁴⁵ ScI	6210.676	3d4s ² 2D	3/2	+8.98	269.2137	-0.88	-26.3817	3d4s(1D)4p 2D	3/2	-11.5	-344.7614	—	—
⁴⁵ ScII	5526.790	3p ⁶ 3d ² 1G	4.0	—	M 135.232	—	M -63.44	3p ⁶ 3d4p 1F ^o	3.0	—	193.1	—	-65
⁴⁵ ScII	5552.224	3p ⁶ 4s ² 1S	0.0	—	—	—	—	3p ⁶ 3d4p 3P ^o	1.0	—	258.0	—	12.0
⁴⁵ ScII	5657.896	3p ⁶ 3d ² 3P	2.0	—	M -27.732	—	M 22.13	3p ⁶ 3d4p 3P ^o	2.0	—	105.6	—	-21
⁴⁵ ScII	5684.202	3p ⁶ 3d ² 3P	2.0	—	-27.2	—	26.0	3p ⁶ 3d4p 3P ^o	1.0	—	258.0	—	12.0
⁴⁵ ScII	6245.637	3p ⁶ 3d ² 3P	2.0	—	M -27.732	—	22.13	3p ⁶ 3d4p 3D ^o	3.0	—	101.8	—	24
⁴⁵ ScII	6300.698	3p ⁶ 3d ² 3P	2.0	—	-27.2	—	26.0	3p ⁶ 3d4p 3D ^o	2.0	—	125.7	—	6.0
⁴⁵ ScII	6320.84	3p ⁶ 3d ² 3P	1.0	—	-108.1	—	-13.0	3p ⁶ 3d4p 3D ^o	1.0	—	307.0	—	1.0
⁴⁵ ScII	6604.601	3p ⁶ 3d ² 1D	2.0	—	149.361	—	7.818	3p ⁶ 3d4p 1D ^o	2.0	—	215.7	—	18
⁵¹ VI	5703.5603d ⁴ (⁵)D)4s a ⁴ D3/2	7.558 ¹	—	2.075 ¹	—	—	—	3d ⁴ (⁵)D)4p y ⁴ F	5/2	—	216.0 ⁵	—	0.0 ⁵
⁵¹ VI	6081.4403d ⁴ (⁵)D)4s a ⁴ D3/2	7.558 ¹	—	2.075 ¹	—	—	—	3d ⁴ (⁵)D)4p z ⁴ P	3/2	—	-286.4 ²	—	-6.0 ²
⁵¹ VI	6090.2203d ⁴ (⁵)D)4s a ⁴ D7/2-160.172 ¹	—	—	15.256 ¹	—	—	—	3d ⁴ (⁵)D)4p z ⁴ P	5/2	—	-89.8 ²	—	8.0 ²
⁵¹ VI	6119.5203d ⁴ (⁵)D)4s a ⁴ D5/2-143.367 ¹	—	—	1.067 ¹	—	—	—	3d ⁴ (⁵)D)4p z ⁴ P	3/2	—	-286.4 ²	—	-6.0 ²
⁵¹ VI	6199.1903d ⁴ (⁵)D)4s a ⁶ D7/2 382.368 ¹	—	—	2.220 ¹	—	—	—	3d ³ (⁴ F)4s4p(³ P ⁰) z ⁶ D 9/2	—	—	503.46 ⁴	—	3.3 ⁴
⁵¹ VI	6243.1003d ⁴ (⁵)D)4s a ⁶ D9/2 406.854 ¹	—	—	14.721 ¹	—	—	—	3d ³ (⁴ F)4s4p(³ P ⁰) z ⁶ D 9/2	—	—	503.46 ⁴	—	3.3 ⁴
⁵¹ VI	6251.8203d ⁴ (⁵)D)4s a ⁶ D7/2 382.368 ¹	—	—	2.220 ¹	—	—	—	3d ³ (⁴ F)4s4p(³ P ⁰) z ⁶ D 7/2	—	—	514.35 ⁴	—	-1.2 ⁴
⁵¹ VI	6274.6503d ⁴ (⁵)D)4s a ⁶ D3/2 405.605 ¹	—	—	-8.060 ¹	—	—	—	3d ³ (⁴ F)4s4p(³ P ⁰) z ⁶ D 1/2	—	—	939.94 ⁴	—	0.0 ⁴
⁵¹ VI	6285.1603d ⁴ (⁵)D)4s a ⁶ D5/2 373.595 ¹	—	—	-2.575 ¹	—	—	—	3d ³ (⁴ F)4s4p(³ P ⁰) z ⁶ D 3/2	—	—	594.69 ⁴	—	-4.4 ⁴
⁶³ CuI	5105.537 4p 2P [case e]	1.5	6.5	194.865	-0.96	-28.78	—	4s2 2D [case b]	2.5	24.97	748.582	6.20	185.871
⁶³ CuI	5218.197 4p 2P [case e]	1.5	6.5	194.865	-0.96	-28.78	—	4d 2D [—]	2.5	0.0*	0.0*	0.0*	0.0*
⁶⁵ CuI	5105.537 4p 2P [case e]	1.5	6.96	208.66	-0.86	-25.78	—	4s2 2D [case b]	2.5	26.79	803.14	5.81	174.18
⁶⁵ CuI	5218.197 4p 2P [case e]	1.5	6.96	208.66	-0.86	-25.78	—	4d 2D [—]	2.5	0.0*	0.0*	0.0*	0.0*

Table A.2: Central wavelengths from NIST or Kurucz line lists and total oscillator strengths from line lists by Kurucz, NIST and VALD, literature, and adopted values. In column 7, literature oscillator strength values are from the following references: 1 Ramírez & Allende Prieto 2011; 2 Lawler et al. (2014).

species	λ (Å)	χ_{ex} (eV)	gf _{Kurucz}	gf _{NIST}	gf _{VALD}	gf _{literature}	gf _{adopted}
⁴⁵ ScI	5671.805/828N	1.447908	+0.640	+0.495	+0.495	—	+0.495
⁴⁵ ScI	5686.826/856	1.439588	+0.530	+0.376	+0.376	—	+0.276
⁴⁵ ScI	6210.676/658	0.000000	-1.570	-1.53	-1.529	—	-1.53
⁴⁵ ScII	5526.790/785	1.768298	+0.13	+0.02	+0.024	—	-0.28
⁴⁵ ScII	5552.224/235	1.455221	-2.270	—	-2.119	-2.28 ¹	-2.27
⁴⁵ ScII	5657.896/907	1.507058	-0.50	-0.60	-0.603	—	-0.60
⁴⁵ ScII	5684.202/214	1.507508	-1.050	-1.07	-1.074	-1.07 ¹	-1.07
⁴⁵ ScII	6245.637/641	1.507508	-0.98	—	-1.030	-1.04 ¹	-1.18
⁴⁵ ScII	6300.698/746	1.507508	-1.840	—	-1.887	-1.95 ¹	-1.99
⁴⁵ ScII	6320.851/843	1.500496	-1.770	—	-1.819	-1.92 ¹	-1.97
⁴⁵ ScII	6604.601/578	1.357044	-1.48	-1.31	-1.309	-1.31 ¹	-1.41
⁵¹ VI	5703.560	1.050919	—	-0.211	-0.211	-0.21 ²	-0.211
⁵¹ VI	6081.440	1.050919	—	-0.578	-0.579	-0.61 ²	-0.578
⁵¹ VI	6090.220	1.080616	—	-0.062	-0.062	-0.07 ²	-0.162
⁵¹ VI	6119.520	1.063602	—	-0.320	-0.320	-0.36 ²	-0.47
⁵¹ VI	6199.190	0.286572	—	-1.28	-1.300	-1.46 ²	-1.48
⁵¹ VI	6243.100	0.300634	—	-0.98	-0.980	-0.94 ²	-0.88
⁵¹ VI	6251.820	0.286572	—	-1.34	-1.340	-1.37 ²	-1.44
⁵¹ VI	6274.650	0.266964	—	-1.67	-1.670	-1.70 ²	-1.72
CuI	5105.537	1.389035	-1.516	-1.50	-1.542	—	-1.52
CuI	5218.197	3.816948	+0.476	+0.26	+0.364	—	+0.0

Table A.3: Hyperfine structure for Cu I lines.

5105.50Å; $\chi=1.39$ eV log gf(total) = -1.520			5218.20Å; $\chi=3.82$ eV log gf(total) = +0.0		
λ (Å)	log gf	iso	λ (Å)	log gf	iso
5105.562	-2.8856	63	5218.195	-1.2041	63
5105.563	-2.9314	63	5218.197	-1.2499	63
5105.554	-2.5634	63	5218.197	-0.8819	63
5105.567	-3.8856	63	5218.201	-2.2041	63
5105.558	-2.8187	63	5218.201	-1.1372	63
5105.540	-2.3135	63	5218.203	-0.6320	63
5105.562	-4.0617	63	5218.206	-2.3802	63
5105.544	-2.9156	63	5218.206	-1.2341	63
5105.516	-2.1075	63	5218.206	0.0	63
5105.565	-3.3619	65	5218.194	-1.2041	65
5105.566	-3.4077	65	5218.196	-1.2499	65
5105.555	-3.0397	65	5218.196	-0.8819	65
5105.570	-4.3619	65	5218.201	-2.2041	65
5105.559	-3.2950	65	5218.201	-1.1372	65
5105.540	-2.7898	65	5218.201	-0.6320	65
5105.564	-4.5380	65	5218.206	-2.3802	65
5105.545	-3.3919	65	5218.206	-1.2341	65
5105.514	-2.5838	65	5218.206	-0.4260	65